Journal of Thermal Analysis and Calorimetry
https://doi.org/10.1007/s10973-026-15957-8

Solar power tower plants: a review on the potentials, requirements, characteristics, and components

Hayder Al-Sarraf[1,2,3] · Ahmed Alhusseny[4,5] · Hassan Mansour Raheem[2,4]

Received: 19 November 2025 / Accepted: 24 June 2026

Abstract
Concentrating solar power (CSP) plants, notably solar power tower (SPT) plants, have significant potential to generate carbon-free electricity. This work briefly overviews CSP technologies, whereas SPT is presented in greater detail. In addition, the essential requirements, solar irradiance, land, water needs, and grid proximity to install a CSP plant are explained. This work highlights the significance of integrating direct steam generation (DSG) technology with SPT plants. Depending on the solar field aperture area, operational DSG-based SPT plants can produce more electricity than molten-salt-based SPT plants. Also, a comprehensive review of SPT plant components and the most relevant literature is presented, along with a classification of their operational status. A research proposal is presented to study the off-design factors affecting the operation of SPT and its components. Hence, the literature reveals a lack of understanding of the effects of these factors on the thermal performance of solar receivers and the overall performance of SPT plants.

Keywords Concentrating solar power · Solar power tower · Direct steam generation · Solar irradiance fluctuation

Abbreviations

CSP	Concentrating solar power
STPP	Solar thermal power plant
SPT	Solar power tower
CRS	Central receiver system
DSG	Direct steam generation
HTF	Heat transfer fluid
TES	Thermal energy storage
GHG	Greenhouse gases
DNI	Direct normal irradiance
HRSG	Heat recovery steam generation
REFOS	Receiver for a fossil-hybrid gas turbine system
LEC	Levelized electricity cost
FPR	Falling particle receiver
SNL	Sandia National Laboratories
PHF	Power to heliostats area factor W m^{-2}

✉ Hayder Al-Sarraf
hayder.al-sarraf@autuni.ac.nz

1 Department of Mechanical Engineering, Auckland University of Technology, Auckland 1142, New Zealand

2 Midland Refineries Company, Ministry of Oil, Karbala Refinery, Karbala 56001, Iraq

3 Department of Fire Engineering, Future Skills Academy, Manukau City Center, Auckland 2104, New Zealand

4 Department of Mechanical Engineering, Faculty of Engineering, University of Kufa, Najaf 54003, Iraq

5 Department of Mechanical and Aerospace Engineering, School of Engineering, University of Manchester, Manchester M13 9PL, UK

Historical perspectives

The need for energy resources has spanned hundreds of years. Such resources are required for several purposes of mankind's usage for the sake of enhancing living conditions and meeting development [1]. These energies have a significant impact on human comfort, including lighting, heating, cooling, and transportation. Electric and thermal energies are more substantial on both domestic and industrial levels [2]. Since the industrial revolution in the nineteenth century, hydrocarbon resource consumption, like coal, oil, and natural gas, has rapidly increased as various types of industries were essentially fossil-fuel-based. Meanwhile, petroleum and natural gas exploration at the time encouraged industry expansion. The literature shows that worldwide energy demand, measured in quadrillion Btu, for different energy resources over the period from 1960 to 2050, has changed rapidly. Notably, until 2020, dependence on fossil fuels was dominant compared to other energy sources. However, global energy scenarios expect a huge reduction in fossil fuel consumption by 2050 [3].

The aggressive use of traditional fossil fuels mainly causes three penalties. First, the price has climbed significantly, especially in recent years, which should be considered from an economic perspective [4]. For instance, one Brent crude oil barrel rose from $42 in 2020 to $71 in 2021, then to $120 in 2022. Likewise, the price of natural gas in the European markets increased 10 times from 2020 to 2021 [3]. Second, it contributes to the depletion of natural resource reserves [5]. Third, it causes global warming due to the high rate of emission of greenhouse gases (GHG) [6]. Consequently, the carbon dioxide (CO_2) content significantly increases [7]. Hence, the CO_2 emitted rose from 10 to 35 BMT from 1960 to 2020. Even though global endeavors to diminish GHG are still active, the rate has progressed in recent years [8]. In addition to the above-mentioned penalties, the stability of procuring fossil fuels is not secured, especially during wars and disputes [9]. As renewable energy sources can be an alternative to fossil fuels [10], they have been in high demand by the international community [11]. The efforts of many countries are evident in transitioning to an alternative energy source that is cost-effective and available year-round. That will help the population meet the increasing energy demand. The most important aspect of the proposed energy source is to be sustainable and reliable [12]. Thus, it can support these countries' development strategies and increase their dependence on clean energy [13]. The latter will create a sustainable economy and new jobs in the renewable energy market. This kind of energy is considered green energy and has no impact on the earth (environmentally friendly). In other words, energy can address environmental challenges.

Renewable energy could be obtained from different sources, such as the sun, wind, hydrogen, and bioenergy [14], geothermal [15], hydropower, etc. In this work, the emphasis will be on solar thermal energy and the plants used to harvest it. For being abundant, environmentally friendly, and inexpensive, solar energy is nowadays considered a promising source of renewable energy [10].

To elaborate further, using solar thermal energy offers several advantages over traditional energy sources, thereby enhancing environmental, operational safety, and long-term energy security. For example, it is a carbon-free energy source that significantly reduces pollution [16]. Furthermore, significant economic benefits can be achieved, particularly when using concentrating solar power plants (CSP) [17]. Yet, the most important incentive is that the Earth receives about four quadrillion kWh of solar thermal energy daily, which is assumed to be more than 10 k times the energy consumed by the world's population [18]. However, the solar energy that reaches the Earth's surface remains low in density and intermittent due to atmospheric attenuation and cloud events. Therefore, to efficiently harness this abundant energy, solar collectors are further improved to capture most of the available solar irradiation through increased concentration [19].

Motivation, scope, and contribution of this review

Why SPT among CSP technologies? Four concentrating solar power (CSP) configurations are currently available at commercial or near-commercial scale: the parabolic trough collector (PTC), the solar power tower (SPT), the linear Fresnel reflector (LFR), and the solar parabolic dish (SPD) [20]. Each technology differs in its optical concentration principle, achievable operating temperature, and suitability for large-scale deployment. PTC and LFR are line-focus technologies with concentration ratios typically in the 70–80 range and operating temperatures limited to approximately 400 °C, which constrain their thermodynamic cycle efficiency. The SPD achieves the highest concentration ratio of any CSP technology, up to 3000, but is limited to small, distributed-scale units and has not demonstrated commercial viability at utility-scale. The SPT, operating on a point-focus principle with concentration ratios between 300 and 1500 and working temperatures routinely exceeding 550 °C, occupies a unique position among CSP technologies: it combines large-scale commercial readiness with the highest thermodynamic efficiency among mature CSP options [21–23]. For these reasons, the present review is deliberately focused on SPT systems, while other CSP technologies are acknowledged in their comparative context.

Limitations of photovoltaic (PV) systems. Although photovoltaic (PV) technology has experienced remarkable cost reductions over the past decade, several fundamental limitations contextualize the continuing relevance of dispatchable CSP systems. PV efficiency declines with increasing panel temperature at a rate of approximately 0.3–0.5% per °C above the standard test condition of 25 °C, a particularly significant penalty in the high-temperature desert environments where SPT plants are most competitive [23]. Furthermore, large-scale PV systems generate electricity only during daylight hours and exhibit rapid output variability under partial cloud cover, imposing substantial ramp-rate challenges on grid operators. Without grid-scale battery storage, which remains costly at the 4-16-h discharge durations required for firm power delivery, PV cannot independently guarantee a dispatchable electricity supply. CSP plants with integrated thermal energy storage (TES), by contrast, can dispatch electricity on demand around the clock, functioning as controllable power plants fueled entirely by solar energy [24, 25]. This fundamental distinction underpins the complementary and enduring role of SPT technology in a balanced renewable energy portfolio.

Gap in the existing literature. A substantial body of CSP review literature exists; however, many comprehensive reviews have focused on PTC systems or on broad multi-technology surveys that treat SPT as one technology among several. Reviews specifically addressing SPT tend to focus either on isolated components, such as heliostats or receivers, or on techno-economic assessments without detailed treatment of working-fluid thermodynamics or off-design operational behavior. The role of direct steam generation (DSG) technology in SPT systems, its performance advantages relative to molten salt HTF, and its sensitivity to solar irradiance variability have received limited integrated treatment in the published review literature. Furthermore, the effect of meteorological off-design factors, including transient cloud events and wind loading on SPT subsystem performance, remains insufficiently synthesized across the existing body of work [22, 23, 25, 26].

Specific contributions of this work. Against this background, the present review makes the following specific contributions: (i) it provides an integrated assessment of DSG-based SPT plants and quantitatively benchmarks their performance against molten-salt-based counterparts using the power-to-heliostat-area factor (PHF) as a common metric derived from publicly available plant data; (ii) it presents a structured and updated classification of worldwide SPT plants according to operational status, HTF type, and cooling method; (iii) it reviews all major SPT receiver architectures, external tubular, cavity, volumetric, and falling particle, with comparative analysis; (iv) it critically examines TES options in the SPT context; and (v) it identifies the specific research gaps related to off-design performance, particularly the effect of fluctuating solar irradiance on receiver thermal behavior and whole-plant performance.

Concentrating solar power (CSP) technologies

A CSP plant represents a renewable solution offering a sophisticated technology that can convert solar irradiance into high-density thermal energy with outstanding effectiveness, especially in territories with high direct normal irradiance (DNI) [27]. They have been pioneering technologies for the last few decades [28]. Such modern technologies use solar thermal energy as a heat source to drive a heat engine.

Solar thermal energy represents the heat source required in the Rankine and Brayton cycles. The solar thermal collector concentrates and applies the solar thermal beam to a small area. The collector-to-receiver area ratio is high, resulting in a high concentration ratio. Then, the exerted thermal power heats the heat transfer fluid (HTF), which is water in the case of integration with direct steam generation (DSG), to transform it into saturated or superheated steam [29]. CSP plants have the potential to occupy the leading position in generating electricity due to their flexibility, and offer obvious solutions for climate change [30]. To better perceive the CSP configuration, its components are divided into three main sections [31]:

1. Solar field: collector systems/mirrors, tracking system, absorbing tubes, heat transfer fluid, pumping and piping system, heat exchangers, backup structure.
2. Thermal energy storage unit: storage media, encapsulation approach, storage tanks, tank insulation.
3. Power block: turbine, condenser, auxiliary boiler, cooling tower.

Requirements of CSP technologies

Several crucial factors must be satisfied to ensure the proper installation of the CSP in a particular region [32]. Hence, the intensity of the sunrays represented in DNI, a sufficient area, the existence of a cooling method, and the proximity of the grid are mandatory, as described below.

Direct normal irradiance (DNI)

DNI is the magnitude of normal electromagnetic energy that reaches the Earth's surface from the sun, minus the diffuse radiation due to scattering through the atmosphere and cloud events. A great value of DNI is needed to ensure that solar-energy-based electric power generation plants perform suitably. The range of DNI, as reported in the literature, is about (1800–2000) kWh m^{-2}year [33]. CSP systems rely solely on DNI to convert solar energy into thermal energy to produce electricity, unlike photovoltaic (PV) systems, which utilize both DNI and diffuse irradiance.

Territory requirements

Large areas are required to install a CSP plant. Hence, it is one of the main factors in selecting the appropriate CSP technology. Likewise, such areas, such as deserts, which often receive high solar irradiance (DNI), should be affordable. For instance, more than 50 k square meters are used to generate one megawatt of electricity with one-hour storage in case of utilizing the central receiver system [32].

Water requirements and water-saving technologies

CSP plants are well-suited to desert and arid regions because of their high direct normal irradiance, but these environments simultaneously impose a critical constraint: water availability. Water is consumed in SPT plants through three principal pathways: steam-cycle make-up water in wet-cooled plants, heliostat mirror washing, and auxiliary system use. The magnitude of each pathway is strongly dependent on the cooling configuration employed.

Wet cooling through an evaporative cooling tower is the most thermodynamically efficient cooling method because it achieves the lowest condenser temperature and pressure, thereby maximizing cycle efficiency. However, it consumes approximately 2240–2800 L of water per MWh of electricity generated in SPT plants [9, 30]. For a representative 100 MWe plant operating 3500 full-load-equivalent hours per year, this implies an annual make-up water demand of approximately 780–980 million litres. In the arid regions where high-DNI SPT sites are concentrated, the Atacama Desert, the Sahara, the Arabian Peninsula, and the Mojave Desert, water availability at this scale is a significant site-selection and operational constraint.

Dry cooling, using air-cooled condenser (ACC) systems, eliminates evaporative water consumption from the power cycle entirely. Because ambient air temperatures are higher than cooling tower water temperatures, the condenser saturation temperature and back pressure are elevated in dry-cooled plants, typically reducing net electricity generation by 3–10% relative to a wet-cooled equivalent, with the largest penalties occurring during peak summer afternoon temperatures, precisely when solar irradiance and generation demand are highest. Despite this efficiency trade-off, dry cooling is increasingly adopted at low-water sites, including Khi Solar One (50 MWe, South Africa), Jülich Solar Tower (Germany), and Shouhang Dunhuang Phase II (100 MWe, China) [34].

Hybrid cooling combines a dry-air-cooled condenser with a supplemental evaporative circuit that is activated during peak ambient temperatures. This approach limits make-up water consumption to 10–30% of an equivalent fully wet-cooled plant while recovering most of the efficiency penalty of pure dry cooling during peak generation hours. Crescent Dunes (110 MWe, USA) employs hybrid cooling as a practical example of this approach [34].

Heliostat mirror washing represents the second major water consumption pathway. Water consumption for washing is approximately 75–150 L per 100 m^2 of mirror surface per washing cycle [22, 34]. For a large SPT plant with 500,000–1500000 m^2 of heliostat aperture area, a single washing cycle consumes 375,000–2250000 L. At a washing frequency of two to four cycles per month in high-soiling environments, annual washing water consumption ranges from 9 to 108 million litres for large plants. Three principal strategies are employed to reduce this consumption. First, waterless dry robotic cleaning systems use automated brushes or compressed-air mechanisms to traverse the heliostat field and remove loosely adhered dust without water; commercial systems have demonstrated reductions in washing water consumption of 70–90%, although their effectiveness is limited for cemented or hygroscopic deposits [22, 34]. Second, soiling-adaptive cleaning scheduling employs predictive algorithms that incorporate local dust-monitoring data, satellite aerosol optical depth measurements, and statistical soiling-rate models to optimize washing frequency and routing, maximizing annual energy output per litre of water consumed. Third, hydrophobic and anti-soiling mirror coatings under active development reduce the adhesion energy of dust particles to the mirror surface, with controlled trials demonstrating soiling rate reductions of 20–40%, potentially extending inter-cleaning intervals and reducing both water and labour costs [22]. When dry cooling is combined with waterless mirror cleaning technologies, the aggregate water intensity of a large SPT plant can be reduced to approximately 0.2–0.3 L per kWh, approximately one-tenth the consumption of a conventionally wet-cooled plant, making SPT technology viable even at sites with severe water scarcity.

Beyond the direct normal irradiance (DNI) requirement, the long-term performance and maintenance economics of SPT plants are substantially influenced by ambient environmental factors, particularly in desert environments where high-DNI sites are concentrated. Three factors warrant specific discussion: heliostat soiling, wind effects, and dust accumulation.

The reflectivity of heliostat mirror surfaces is a critical driver of field optical efficiency and degrades continuously due to the deposition of particulate matter, including mineral dust, biological material, and industrial aerosols. Clean-mirror specular reflectivity is typically 0.93–0.95; field measurements at operational SPT sites in arid regions of the southwestern United States, the Middle East, and North Africa have recorded reflectivity losses of 0.5–2.0% per day in high-dust environments [22, 34]. If cleaning is performed only weekly, cumulative soiling can reduce field optical efficiency by 5–15%, representing a substantial penalty on annual energy yield. Optimal cleaning scheduling, balancing water consumption and labour cost against the optical performance penalty of delayed intervention, is an active area of operational optimization in the industry. Dry robotic cleaning systems have been developed specifically to reduce water consumption for washing at arid sites.

Wind loading is a primary structural design constraint for heliostat reflector panels and their support structures. At operational SPT sites, sustained wind speeds regularly reach 10–15 m s^{-1}, and storm events can exceed 30–40 m s^{-1}, requiring heliostats to be driven to a protective stow position. At intermediate wind speeds within the operational range, heliostat tracking accuracy is degraded by structural vibration and elastic deformation of the mirror panel and support arm, introducing pointing errors that reduce the fraction of reflected radiation intercepted by the receiver aperture and increase spillage losses. Studies have estimated that sustained wind speeds of 5–8 m s^{-1}can degrade heliostat tracking accuracy by 1–3 mrad, relative to a design requirement of less than 1 mrad RMS, with corresponding reductions in annual optical efficiency of 1–3% at windy sites [35, 36]. Additionally, wind-induced forced convection from external receiver surfaces is a significant thermal loss mechanism; the convective heat loss coefficient scales approximately with the 0.6–0.8 power of wind speed [37], making high-wind sites systematically less favourable for external receiver designs relative to enclosed cavity configurations.

Dust accumulation on receiver surfaces and optical components compounds the soiling effects described above. In volumetric receivers of open-loop configuration, airborne particulate matter deposits within the porous absorber matrix, progressively reducing effective porosity and altering the absorber's pressure drop characteristics, thereby disrupting the designed airflow distribution. In pressurized volumetric receivers with glass windows, dust deposits on the external window surface reduce optical transmissivity. In falling particle receivers, atmospheric dust can contaminate the particle inventory, altering its optical absorptance and thermophysical properties over extended operation [25, 38]. Receiver cleaning protocols and aperture design features, such as air curtain or purge-flow systems, are incorporated in advanced receiver designs to mitigate particulate ingress and surface deposition.

Access to network equipment

Large-scale CSP plants producing megawatt-scale output are deemed to use the same infrastructure as conventional power plants, since both generate high-voltage electricity. The generated electricity will be delivered to consumers via transmission lines. These lines are a key component of determining the location of CSP plants. All these considerations will help minimize operating and maintenance costs. Therefore, it is recommended that more than one plant be installed in the same location [39].

CSP technologies

As mentioned earlier, CSP systems are deployed worldwide and available in different phases in terms of operational, under construction, and development [40]. Nevertheless, of all CSP technologies, SPT has higher advantages as listed below:

1. The mean annual efficiency of solar-to-electric conversion of the plant is (23–35)%, along with a remarkably high field operating temperature [21].
2. Potential of utilizing different conversion cycles: Rankine cycle (RC), Brayton cycle (BC), combined cycle (CC) [22].
3. Considered as large-scale electric power generation plants with a range of (10–200) MW [41].
4. The capacity factor per annum is 55% with thermal energy storage technology (10 h) [24].
5. Higher possibility to reduce costs and increase efficiency. As a result, an affordable levelized electricity cost (LEC) is expected [22]. Hence, it is expected to operate for more than 4500 h annually.
6. The expectation of improvement is very significant [23].
7. High concentration ratio (300–1500) leading to a higher temperature range (150- above 2000 °C) [42].
8. The least expensive technology in comparison with other CSP families for producing electricity [43].
9. The required cooling water is less (2240–2800) l/MWh, whereas parabolic trough collectors and linear Fresnel collectors need (3000–3500) l/MWh and (2900–3500) l/MWh, respectively [9].
10. In comparison with the parabolic trough collector (PTC), the solar power tower (SPT) gives the peak thermodynamic efficiency [30].

Additionally, integrating DSG with SPT further boosts efficiency. Such technology converts water from liquid to steam directly throughout the solar receiver. Then, the steam generated is used to drive the power unit to produce electricity. The beauty of this technology is its capability to raise the temperature of water/steam beyond the maximum limit that synthetic oil temperature can reach [44]. In SPT plants, employing DSG is proven to be cost-effective compared to using synthetic oil with heat exchangers [45]. DSG represents a promising technology with high potential to reduce the complications associated with SPT plants. The most important reasons for employing the DSG technique are listed below [46]:

1. Eliminating the synthetic heat transfer fluid (HTF).
2. No heat exchanger is required, nor is oil used to transfer thermal energy.
3. Simple configuration leads to low maintenance and operation costs (O&M). Thus, lower levelized electricity costs.
4. A higher temperature is achieved (above 400 °C) while synthetic oil degrades at this temperature. Therefore, higher thermodynamic temperatures and overall plant efficiencies are achieved.
5. No environmental hazards (eco-friendly) in case of leakage or fire circumstances.

The benefits, however, come with some technical challenges when using water inside the receiver. For instance, corrosion occurs if the water used is not well purified. Also, the climate conditions significantly affect DSG performance, especially during cloud events. Likewise, in DSG, the SPT plant output is controlled by the sun's availability [47].

Solar power tower (SPT)

SPT is a mature CSP technology that has received considerable attention over the last four decades in the development of high-capacity solar thermal power plants (STPPs). The solar tower has been investigated and studied throughout demonstrated and pilot plants worldwide.

General layout and working principle of SPT plants

The general layout of an SPT plant, illustrated schematically in Fig. 1 [22, 48], consists of five principal subsystems arranged to form a continuous solar-to-electrical energy conversion chain. The heliostat field surrounds the central tower and is designed to maximize the annual optical energy intercepted and reflected onto the receiver aperture. Hence, such a field consists of hundreds of mirrors mounted in circular arrays. These mirrors are individually constructed on a 2-axis tracking system to follow the sun from dawn to dusk. The function of these mirrors is to receive, concentrate, and reflect the incident solar radiation beam onto the solar receiver. The typical heat flux reflected from heliostats to the receiver is (200–1000) kW m^{-2}. However, it depends on the mirror's reflectivity, or, in other words, its optical performance. The receiver, mounted at the top of the tower, absorbs the concentrated solar flux and transfers thermal energy to the circulating heat transfer fluid (HTF) [49]. Depending on the HTF selected, the thermal circuit either feeds a steam generator (for molten salt or synthetic oil) or directly produces steam within the receiver (for DSG). Heat transfers to the HTF throughout the receiver tube wall by conduction and convection. The receiver is made of specific materials subject to high-density heat flux and continuous temperature fluctuations, which cause thermal stresses [50]. Therefore, it should be manufactured from thermal-stress-resistant materials to withstand the substantial solar flux encountered across a wide range of temperatures. Nowadays, receivers are made of metal alloys or ceramics. Thus, reliability, economy, and safety should be considered during the receiver design phase. The HTF thermal circuit connects to the thermal energy storage (TES) system, which decouples electricity generation from the instantaneous availability of solar irradiance. The power conversion block, consisting of a steam or gas turbine, generator, condenser, and associated auxiliaries, converts stored or directly transferred thermal energy into electrical power for grid delivery [22, 51]. The energy conversion chain within an SPT plant proceeds through four sequential stages: (1) optical concentration, in which the heliostat field redirects and concentrates direct normal irradiance (DNI) onto the receiver aperture; (2) solar-to-thermal conversion, in which the receiver absorbs the concentrated flux and heats the HTF; (3) thermal storage and dispatch, in which the TES system buffers energy supply against demand variability; and (4) thermal-to-electrical conversion, in which the power block produces grid-quality electricity. Understanding this chain is essential for identifying where thermodynamic losses occur and where

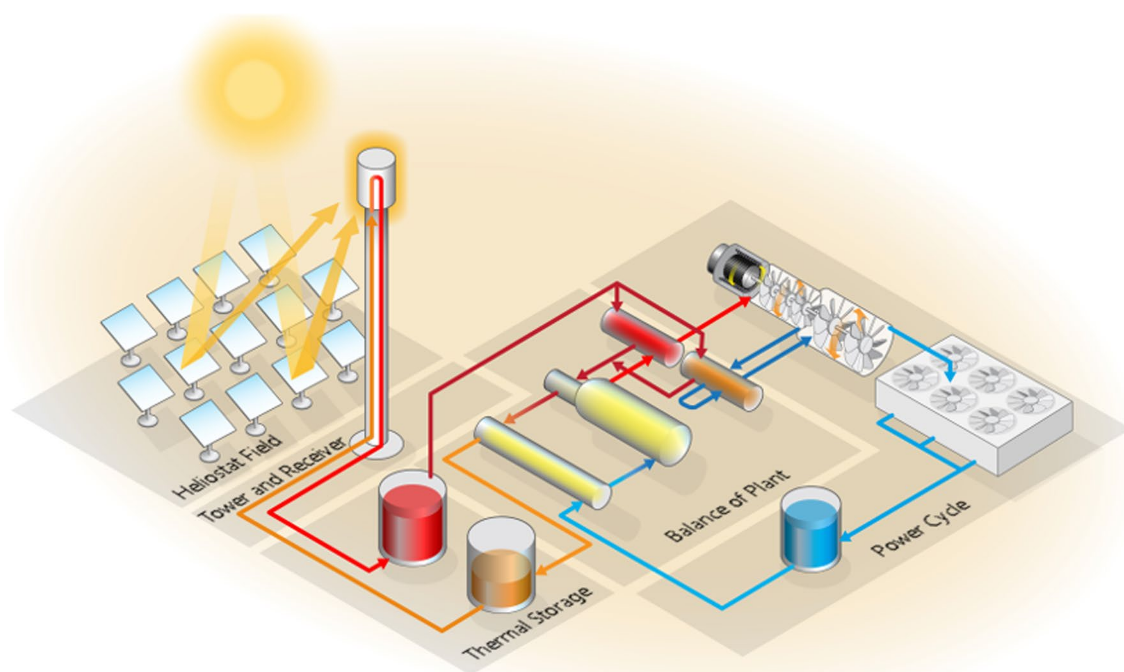

Fig. 1 Schematic layout of a generic Solar Power Tower (SPT) plant illustrating the principal subsystems and energy flow path

performance improvement opportunities are greatest [22, 48].

The feasibility of constructing large-scale solar power tower plants has been demonstrated by the Solar One plant, established in 1982 in the United States. At that time, it was considered the world's largest SPT power generation plant, with 10 MWe [52]. Then, the Solar Two plant was built in California next to the Solar One plant. In 1996, the Department of Energy (DOE) modified the Solar One plant design to validate the use of nitrate salts. SPT technology was also introduced in Sevilla, Spain, with the construction of Planta Solar 10 (PS10) and Planta Solar 20 (PS20). These plants can generate 11 MWe and 20 MWe of electricity, respectively. The integration of thermal energy storage technology with standalone SPT plants is highly significant for maximizing the annual capacity factor [39]. Economically, the rate of electric power generated by SPT is deemed affordable for consumers if the capacity is very large (greater than 10 MWe) [53]. Furthermore, SPT plants would be used for other applications, such as desalination, to produce clean drinking water. Such usage is beneficial, especially in coastal cities and islands with drinking water scarcity, for instance, in Greece and Cyprus [54]. Likewise, generating hydrogen by using a chemical reactor plant is achievable [55]. Significant research on SPT plants has been conducted since 1980. Table 1 presents examples of SPT pilot plants since the 1980s.

As mentioned earlier, SPT can accommodate a wide range of HTFs with different power cycles (Rankine, Brayton, or combined) [34], as shown in Table 2. This represents one of the favorite features, enabling investors/decision-makers to have more freedom in differentiating among various HTFs. Nevertheless, each HTF has characteristics and advantages that may apply to one project but not to another. In other words, determining a specific HTF depends on factors such as project location and climatic conditions. For instance,

Table 1 Samples of SPT pilot plants [48]

Project name	Power/MW	Year to start	TES	HTF	Country
SSPS	0.5	1981	Yes	Liquid sodium	Spain
EURELIOS	1	1981	Yes	Steam	Italy
SUNSHINE	1	1981	Yes	Steam	Japan
Solar One	10	1982	Yes	Steam	USA
CESA-1	1	1983	Yes	Steam	Spain
MSEE/CAT B	1	1984	Yes	Molten nitrate	USA
THEMIS	2.5	1984	Yes	Hi-Tec salt	France
SPP-5	5	1986	Yes	Steam	Russia
TSA	1	1993	Yes	Air	Spain
Solar Two	10	1995	Yes	Molten salt	USA

atmospheric air can be utilized to attain high efficiency and quick startup, such as J *ü* lich Solar Tower in Germany [56]. In turn, molten salt has been proven commercially in operational plants such as the Gemasolar Thermosolar Plant in Spain, NOOR III in Morocco, and the Hami 50 MW CSP Project in China.

Table 2 displays the most recent SPT plants and their classification according to the following status: not operational, operational, under construction, and development [34].

It is observed from Table 2, two cooling methods are used in SPT plants: wet and dry. Distinguishing between those kinds depends on how residual heat is extracted from the steam leaving the expansion turbine. Hence, for SPT plants employing wet cooling, water is used to cool down and condense the steam inside a condenser. Then the condensate water is drawn again by a pump for reuse in the plant cycle. The cooling water becomes hot as it absorbs heat inside the condenser and dissipates thermal energy throughout a cooling tower. Such a cooling method is efficient and effective, but has potential drawbacks. It demands high water quantities and delivers high temperatures. On the other hand, the dry-cooling method uses air to cool the steam in SPT plants. A heat exchanger is required for dry cooling to enable the heat exchange between steam and air. Dry cooling is less efficient than wet cooling and is more expensive to install and operate. Finally, combining the two cooling types above yields a hybrid cooling method.

Heat transfer fluids in SPT plants: types, properties, and commercial deployment

The selection of the heat transfer fluid (HTF) is one of the most consequential design decisions in an SPT plant, as it governs the achievable operating temperature, thermodynamic cycle efficiency, TES strategy, environmental risk, and capital and operational costs. The following subsections review the principal HTF categories employed or investigated for SPT applications, and Table 3 provides a comparative summary of their key thermophysical properties and deployment status.

Water/Steam (Direct steam generation)

Water is the working fluid in the Rankine cycle and, when used as HTF directly within the solar receiver, constitutes the DSG configuration. DSG eliminates the need for a separate HTF circuit and its associated heat exchangers, simplifying plant layout and reducing heat-exchange losses. Operating pressures in DSG-SPT systems are typically 40–160 bar, with steam temperatures reaching 400–550 °C [46]. The principal thermophysical advantage of water as HTF is its exceptionally high latent heat of vaporization,

Table 2 SPT plants in multiple statuses (not operational, operational, under construction, under development) [34]

Project name	Year to start	Country	Net power (MW)	Gross power (MW)	Status	HTF	Cooling method	TES
Solar One	1982	USA	10	10	Not Operational	Water	N/A	Oil/ rock
Solar Two	1995	USA	10	10	Not Operational	Molten salt	N/A	Nitrate salt
Sierra SunTower	2009	USA	5	5	Not Operational	Water	Wet cooling	None
Lake Cargelligo	2011	Australia	3	3	Not Operational	Water/Steam	N/A	Core graphite
National Solar Thermal Test Facility	1976	USA	5	5	Operational	Molten salt	N/A	N/A
Planta Solar 10	2007	Spain	11	11.02	Operational	Water	Wet cooling	Other
Julich Solar Tower	2008	Germany	1.5	1.5	Operational	Air	Dry cooling	Other
Planta Solar 20	2009	Spain	20	20	Operational	Water	Wet cooling	Other
Supcon Solar Project	2018	China	50	50	Operational	Molten salt	N/A	2- Tank direct
ACME Solar Tower	2011	India	2.5	2.5	Operational	Water/Steam	Wet cooling	None
Gemasolar Thermosolar	2011	Spain	19.9	19.9	Operational	Molten salt	Wet cooling	2- Tank direct
Dahan Power Plant	2012	China	1	1	Operational	Water/Steam	Wet cooling	Other
Greenway CSP Mersin	2012	Turkey	1.4	1.4	Operational	Water	N/A	Other
CRS Sales	2012	Spain	5	5	Operational	Molten salt	N/A	N/A
Ivanpah Solar Electric	2014	USA	377	392	Operational	Water	Dry cooling	None
SUPCON Delingha	2013	China	10	10	Operational	Water	Wet cooling	2- Tank direct
Crescent Dunes	2015	USA	110	110	Operational	Molten salt	Hybrid	2- Tank direct
Jemalong Solar Thermal	2016	Australia	N/A	1.1	Operational	Liquid Sodium	Dry cooling	2- Tank direct
Khi Solar One	2016	South Africa	50	50	Operational	Water	Dry cooling	Other
Sundrop CSP Project	2016	Australia	1.5	1.5	Operational	Water	N/A	None
Qingha Gonghe	2016	China	50	50	Operational	Molten salt	Dry cooling	2-Tank direct
Ashalim Plot B	2017	Israel	121	121	Operational	Water	N/A	None
NOOR III	2018	Morocco	150	150	Operational	Molten salt	N/A	2- Tank direct
Hami	2019	China	50	50	Operational	Molten salt	N/A	2- Tank direct
SEDC	2008	Israel	6	6	Operational	Water	N/A	N/A
Shouhang Dunhuang I	2016	China	10	10	Operational	Molten salt	N/A	2- Tank direct
Shouhang Dunhuang II	2018	China	100	100	Operational	Molten salt	Dry	2- Tank direct
LuNeng Haixi	2019	China	50	50	Operational	Molten salt	N/A	2- Tank direct
Atacama-1	2018	Chile	110	110	Under construction	Molten salt	N/A	2- Tank direct
Golmud	2018	China	200	200	Under construction	Molten salt	N/A	2- Tank direct
Noor Energy1 / DEWA IV	2022	UAE	100	100	Under construction	Molten salt	N/A	2-Tank direct
Yumen 50	N/A	China	50	50	Under construction	Molten salt	N/A	2- Tank direct
Redstone	2023	South Africa	100	100	Under construction	Molten salt	Dry cooling	2- Tank direct
Golden Tower	2016	China	100	100	Under development	Molten salt	N/A	2- Tank direct
Copiapó	2019	Chile	260	260	Under development	Water/Steam	Dry cooling	2- Tank direct
Shangyi 50 MW DSG Tower CSP Project	N/A	China	50	50	Under development	Water/Steam	N/A	2- Tank indirect

Table 3 Comparative thermophysical properties and deployment status of HTFs used in SPT plants [22, 25, 34, 44, 46, 47, 57, 58]

HTF	Operating temp. range/°C	Specific heat/ kJ kg^{-1} K^{-1}	Thermal conductivity/W m^{-1} K^{-1}	Density/kg m^{-3}	TES compatibility	Commercial SPT use
Water/ Steam (DSG)	100–550	4.18 (liquid)/2.1 (steam)	0.6 (liquid)	958 (100 °C, liquid)	Steam accumulator	Yes, Ivanpah, Khi Solar One, Ashalim
Molten Salt (Solar Salt)	220–565	1.50	0.50	1900 (300 °C)	Direct two-tank	Yes, Gemasolar, NOOR III, Crescent Dunes
Synthetic Oil (Therminol VP-1)	15–400	2.10	0.12	870 (300 °C)	Indirect two-tank	No, used primarily in PTC
Air	Ambient, > 1000	1.0	0.03–0.07	0.6 (300 °C)	Solid media TES	Pilot only, Jülich, Germany
Liquid sodium	100–880	1.27	70 (400 °C)	850 (400 °C)	Two-tank	Very limited, Jemalong, Australia

approximately 2257 kJ kg^{-1} at 100 °C, decreasing with increasing pressure, which enables efficient enthalpy uptake in the boiling section of the receiver. Its specific heat capacity in the liquid phase is approximately 4.18 kJ kg^{-1}·K, and its thermal conductivity is approximately 0.6 W m^{-1} K^{-1} at near-ambient conditions, yielding convective heat transfer coefficients during nucleate boiling that are among the highest achievable in any HTF configuration [44, 46]. Water is non-toxic, non-flammable, and abundantly available, making it environmentally benign. However, DSG operation introduces two-phase flow complexity, with distinct preheating, evaporation, and superheating zones within a single receiver, making flow control and thermal uniformity challenging, particularly during transient cloud events and at partial load [26, 47]. DSG technology has been commercially proven at large scale in several major operational plants, including the Ivanpah Solar Electric Generating System (377 MWe, USA), Khi Solar One (50 MWe, South Africa), and Ashalim Plot B (121 MWe, Israel).

Molten salt

Molten nitrate salt, most commonly a binary mixture of 60 mass% $NaNO_3$ and 40 wt% KNO_3, commercially known as Solar Salt, is the most widely deployed HTF in large-scale commercial SPT plants. It operates as a liquid over the temperature range of approximately 220–565 °C. Its key thermophysical properties at 300 °C include a specific heat capacity of approximately 1.5 kJ kg^{-1} K^{-1}, a density of approximately 1900 kg m^{-3}, and a thermal conductivity of approximately 0.5 W m^{-1}K^{-1} [34, 57]. The primary advantage of molten salt is its ability to serve simultaneously as HTF and TES medium in a direct two-tank storage configuration, eliminating the heat exchanger between the solar field and the storage system and significantly improving round-trip storage efficiency. Molten salt SPT technology is commercially proven in plants including Gemasolar (19.9 MWe, Spain), Crescent Dunes (110 MWe, USA), NOOR III (150 MWe, Morocco), and DEWA/Noor Energy 1 (100 MWe, UAE) [34]. The principal limitation of molten salt is its relatively high freezing point, approximately 220 °C for Solar Salt, necessitating freeze protection through trace heating during night-time and low-irradiance periods, adding parasitic energy consumption and operational complexity. Research into advanced ternary and quaternary nitrate/nitrite salt formulations aims to reduce the minimum operating temperature below 100 °C to mitigate this challenge [25].

Synthetic thermal oil

Synthetic thermal oils, most notably Therminol VP-1 and Dowtherm A, both eutectic biphenyl/diphenyl oxide mixtures, have been extensively used as HTFs in PTC plants and studied as candidates for SPT applications. These oils operate in the liquid phase over a temperature range of approximately 15–400 °C, beyond which thermal cracking and irreversible chemical degradation occur [44, 45]. Their thermophysical properties at 300 °C include a specific heat capacity of approximately 2.1 kJ kg^{-1} K^{-1}, a density of approximately 870 kg m^{-3}, and a thermal conductivity of approximately 0.12 W m^{-1} K^{-1}, which are notably lower than those of molten salts, implying higher thermal resistance in receiver tubes [57]. The vapor pressure of synthetic oils is relatively high at elevated temperatures, reaching approximately 10 bar at 400 °C, requiring pressurized piping systems that add to plant costs and complexity. In SPT applications, oil would be used in an indirect two-tank TES configuration with a separate oil-to-salt heat exchanger, which introduces additional thermodynamic irreversibilities and capital costs. Furthermore, synthetic oils are flammable and present environmental risks in the event of a leak, requiring secondary containment systems. For these reasons, synthetic oil has not been deployed as the primary HTF in any large-scale commercial SPT plant; however, it provides a relevant technology reference against which DSG and molten salt are benchmarked, and it remains of interest for hybrid mid-temperature SPT configurations [45, 57].

Air

Atmospheric and pressurized air are used as HTF in volumetric receiver configurations, particularly in open-loop and closed-loop (pressurized) arrangements coupled with Brayton or combined power cycles. Air can operate over an extremely wide temperature range, potentially exceeding 1000 °C in pressurized volumetric receiver demonstrations [58, 59], and is non-toxic, non-corrosive, and freely available. However, its thermophysical properties are comparatively poor: a specific heat capacity of approximately 1.0 kJ kg^{-1} K^{-1} and a thermal conductivity of approximately 0.03 W m^{-1} K^{-1} at ambient conditions, which improve with temperature but remain far below those of liquid HTFs. The low air density necessitates high volumetric flow rates and imposes significant pressure drop penalties in receiver systems. Air does not permit direct TES in conventional two-tank systems; instead, high-temperature solid TES media must be used. The Jülich Solar Tower (1.5 MWe, Germany) is the most established pilot-scale demonstration of air-based SPT technology [56].

Liquid sodium

Liquid sodium has been investigated as an HTF for SPT receivers due to its exceptionally high thermal conductivity of approximately 70 W m^{-1} K^{-1} at 400 °C, which enables very high convective heat transfer coefficients and potentially more uniform receiver tube wall temperatures under non-uniform solar flux distributions. Its operating temperature range is approximately 100–880 °C, and its specific heat capacity is approximately 1.27 kJ kg^{-1} K^{-1} [22, 57]. However, liquid sodium is highly reactive with water and air, posing severe safety risks: any leak in a sodium-based HTF circuit can cause violent combustion or an explosion upon contact with moisture. This intrinsic hazard has severely limited commercial adoption. The Jemalong Solar Thermal Station (1.1 MWe, Australia) is among the few operational SPT plants to have employed liquid sodium as HTF [34].

Techno-economic comparison: DSG versus molten salt

The choice between DSG and molten salt as HTF involves trade-offs that extend beyond thermophysical properties to include capital cost, levelised cost of electricity (LCOE), operational complexity, and storage flexibility. Recent quantitative assessments provide the following representative benchmarks [22, 25]:

Regarding LCOE, molten-salt SPT plants with two-tank TES have demonstrated values of 0.12–0.18 USD kWh^{-1} in recent commercial projects, Crescent Dunes at approximately 0.135 USD kWh^{-1}, and NOOR III at approximately 0.15 USD kWh^{-1}, depending on storage capacity and site DNI. DSG-SPT plants without TES, such as Ivanpah, have reported LCOE values of approximately 0.13–0.20 USD kWh^{-1}, but their capacity factors are inherently limited by the absence of dispatchable storage. Regarding capacity factor, molten-salt SPT plants with 10–15 h of TES achieve annual capacity factors of 55–75%, compared to 25–35% for DSG plants without storage. In terms of capital cost, the two-tank molten salt TES system adds approximately 80–120 USD/kWh_{th} to the total capital expenditure, while DSG eliminates the HTF loop and its associated heat exchangers, reducing solar field piping costs by an estimated 10–20% relative to indirect molten-salt configurations. Regarding irradiance variability sensitivity, DSG systems are more sensitive to rapid irradiance transients because the two-phase flow regime within the receiver responds immediately to flux changes, leading to instability in steam quality and pressure. Molten salt's larger thermal mass and single-phase flow characteristics provide a natural buffer against short-duration cloud events, though prolonged low-DNI periods still require energy input for freeze protection [26, 47]. On balance, molten salt with two-tank TES currently represents the preferred commercial choice for utility-scale SPT plants requiring high capacity factors and firm dispatchability. DSG remains competitive in applications where storage is not required or where plant simplicity and lower HTF water costs are decisive factors.

Operational SPT plants producing significant amounts of electricity are limited worldwide. In addition, not all technical data required to differentiate among such plants is publicly accessible. Therefore, in this work, the analysis will be based on the PHF concept for the currently operational SPT plants. PHF is calculated as follows.

$$PHF = \frac{\text{Electric Power Genrated (W)}}{\text{Aperture Area}\ \left(m^2\right)}$$

The *ElectricPowerGenrated* represents the magnitude of electricity produced by the SPT plant and delivered to the grid in watts. The *ApertureArea* represents the heliostats' surface area in m^2, which receives, concentrates, and reflects the downwelling sunlight. Employing the PHF concept, typically measured in (W m^{-2}), is a beneficial tool for a preliminary comparison among SPT plants based on the HTF used. However, additional key parameters are still required to assess SPT plant performance, efficiency, and cost-effectiveness. Therefore, the PHF concept can be used for the theoretical comparison, while the collector efficiency, HTF quality, and overall design of the SPT plant are used for the practical comparison. Additionally, using the PHF concept to compare SPT plants will provide useful information on HTF thermal performance, which is essential for determining the amount of heat conveyed from the solar receiver to the power block. Higher PHF values lead to higher electric power generation per unit area, which is desirable, especially in limited territories. Table 4 highlights PHF to compare the performance of SPT plants with production capacity above 10 MWe using different HTFs.

Notably, operational SPT plants coupled with DSG generally exhibit the highest PHF levels compared to those based on molten salt. That is due to water's significantly high latent heat of vaporization, as shown in Fig. 2. A plausible conclusion from the above investigation is that SPT integrated with DSG can produce higher electrical power. Again, using water as a cooling fluid has shortcomings, which should be addressed to ensure smooth operation.

Design aspects of solar power tower plants

The engineering design of an SPT plant involves several interrelated sub-problems that must be solved simultaneously to achieve the maximum annual energy output at the minimum cost. The principal design parameters are discussed below.

Heliostat field layout and optimization

The heliostat field layout determines the plant's optical efficiency. Heliostat positions are optimized to maximize the annual reflected energy delivered to the receiver aperture while minimizing blocking, the obstruction of one heliostat by another in the beam path to the receiver, and shading, defined as the shadow cast by one heliostat onto an adjacent mirror's reflective surface. Common field geometries include the surrounding (north–south symmetric) layout, typically adopted at low to mid latitudes, and the north-biased field, more common at higher latitudes where the solar elevation is predominantly to the south during the operational period. The cosine factor, defined as the cosine of the angle between the heliostat normal and the bisector of the sun-heliostat-receiver angle, is the dominant single optical loss mechanism and is minimized by placing heliostats close to the tower, balanced against the blocking and shading penalties that increase with field density [22, 48, 60]. Optimization tools such as DELSOL, HFLCAL, and SolarPILOT are widely used for field layout design, iteratively adjusting mirror positions, field radius, and angular density to maximize the annual solar multiple for a given aperture area and tower height.

Tower height

The tower height is selected as a function of the heliostat field radius. As the field radius increases to accommodate larger installed capacity, the tower must be proportionally taller to maintain an acceptable incidence angle at

Table 4 PHF of operational SPT plants producing more than 10 MWe with different HTF

Plant name	HTF	Power/MW_e	Aperture area m^{-2}	PHF/W m^{-2}
Planta Solar 10	Water	11	75,000	146.66
Planta Solar 20	Water	20	150,000	133.33
Supcon Solar Project	Molten salt	50	542,700	92.13
Gemasolar Thermosolar Plant	Molten salt	20	304,750	65.62
Ivanpah Solar Electric Generating System	Water	377	2,600,000	145
Crescent Dunes Solar Energy Project (Tonopah)	Molten salt	110	1,197,148	91.88
Khi Solar One	Water	50	576,800	86.68
Qingha Gonghe 50 MW	Molten salt	50	516,000	96.89
Ashalim Plot B	Water	121	1,052,480	114.96
NOOR III	Molten salt	150	1,312,000	114.32
Hami 50 MW CSP Project	Molten salt	50	696,751	71.76
LuNeng Haixi	Molten salt	50	610,000	81.96
Shouhang Dunhuang Phase I	Molten salt	10	175,375	57.02
Shouhang Dunhuang Phase II	Molten salt	100	1,400,000	71.42
SUPCON Delingha	Water	10,000	63,000	158.73

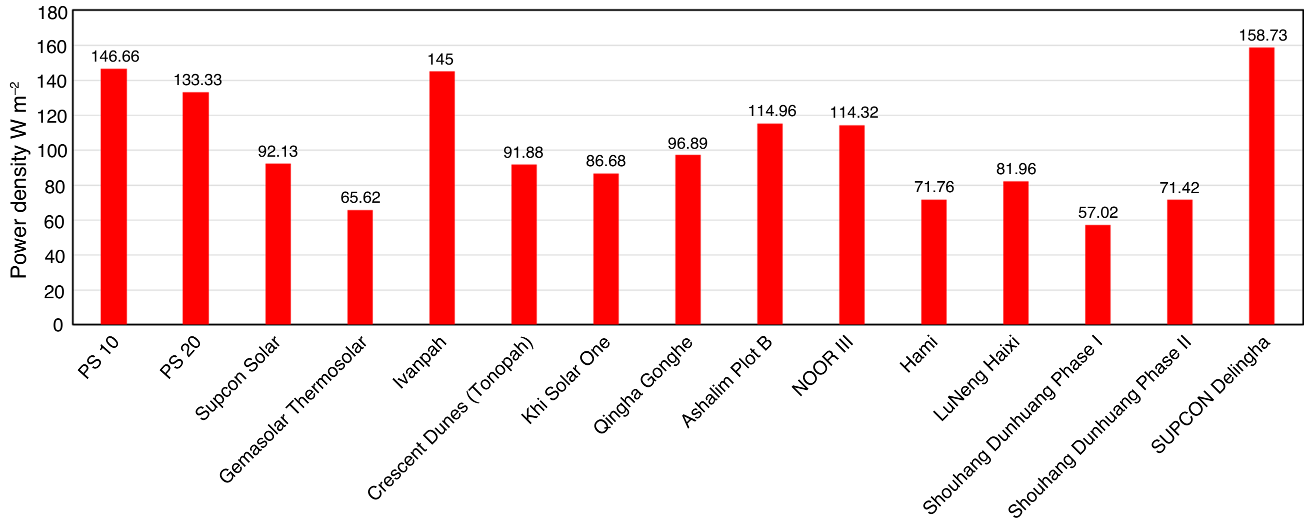

Fig. 2 PHF for different SPT plants operating beyond 10 MWe with various HTFs

the outermost heliostats and to limit beam spillage at the receiver aperture.

Receiver sizing and aperture area

The receiver aperture area is defined to intercept a targeted fraction of the reflected radiation, typically 95–98% of the designed peak flux, while minimizing the re-radiation, convective, and reflective losses that scale with receiver external surface area. For a given solar multiple, the receiver aperture is determined by the peak concentrated flux and the allowable maximum tube wall temperature, which is constrained by the HTF thermal stability limit and the tube material's creep resistance. Tube diameter, wall thickness, and panel arrangement are then derived from heat transfer and structural mechanics considerations, ensuring that the peak heat flux does not exceed the HTF's critical heat flux and that thermal stresses remain within the fatigue life limits of the tube material [50, 61].

Solar multiple and thermal energy storage sizing

The solar multiple (SM) is defined as the ratio of the solar field's installed thermal power to the power block's rated thermal input at design-point conditions. An SM of 1.0 implies that at the design-point DNI, the solar field exactly meets the turbine's thermal demand, with no surplus for charging storage. Commercial SPT plants with TES are typically designed with solar multiples of 2.0–3.0, enabling both full-power turbine operation during peak solar hours and concurrent TES charging [24, 25]. TES capacity is expressed in equivalent full-load hours and is sized to satisfy the intended dispatch schedule. Plants targeting baseload-equivalent operation with capacity factors exceeding 60% require approximately 10–15 h of TES, achieved with a solar multiple in the range of 2.5–3.0 [24, 25]. The combined optimization of solar multiple and TES capacity is performed using annual simulation tools, such as the System Advisor Model (SAM), to minimize LCOE, subject to local DNI, land availability, and grid dispatch requirements.

Energy and exergy analysis framework for SPT systems

A rigorous thermodynamic assessment of SPT plants requires both energy (first law) and exergy (second law) analysis. The energy model quantifies the magnitude of thermal losses at each conversion stage, while the exergy model identifies the thermodynamic quality of those losses, that is, their irreversibility, and pinpoints the subsystems with the greatest potential for efficiency improvement.

Energy model

The overall plant energy efficiency, ζ_{plant} is expressed as the product of the efficiency factors governing each conversion stage in the energy chain:

$$\zeta_{\text{plant}} = \zeta_{\text{field}} \times \zeta_{\text{receiver}} \times \zeta_{\text{HTF}} \times \zeta_{\text{TES}} \times \zeta_{\text{PB}}$$

where ζ_{field} is the heliostat field optical efficiency, accounting for cosine losses, blocking, shading, atmospheric attenuation, and mirror reflectivity losses; ζ_{receiver} is the receiver thermal efficiency; ζ_{HTF} accounts for piping and pumping losses in the HTF circuit; ζ_{TES} is the round-trip efficiency of the thermal energy storage system; and ζ_{PB} is the thermal efficiency of the power block (Rankine or Brayton cycle) [22, 62].

The receiver thermal efficiency is the most sensitive parameter in this product and is expressed as:

$$\zeta_{receiver} = \frac{Q_{absorbed}}{Q_{incident}}$$

where $Q_{incident}$ is the total concentrated solar power impinging on the receiver aperture; $Q_{absorbed}$ is the net thermal power transferred to the HTF. $Q_{absorbed}$ is expressed as:

$$Q_{absorbed} = Q_{incident} - Q_{rad} - Q_{conv} - Q_{ref}$$

where Q_{rad} is the re-radiation heat loss from the receiver surface, proportional to $\in, \sigma, T^4$; Q_{conv} is the convective heat loss to the ambient, dependent on wind speed and receiver geometry; and Q_{ref} is the fraction of incident solar power reflected by the receiver surface without absorption [61, 62].

For DSG-based receivers, the power gain ($\dot{Q}_{HTF}$) of the HTF across the three thermodynamic zones, preheating, evaporation, and superheating, is expressed as:

$$\dot{Q}_{HTF} = \dot{m} \times \left(h_{out} - h_{in}\right)$$

where $\dot{m}$ is the mass flow rate of water/steam, and h denotes specific enthalpy at the respective receiver inlet and outlet conditions. For molten salt as HTF, the sensible heat gain is:

$$\dot{Q}_{HTF} = \dot{m} \times C_p \times \left(T_{out} - T_{in}\right)$$

where C_p is the temperature-dependent specific heat capacity of the salt, and T_{out} and T_{in} are the receiver outlet and inlet temperatures, respectively [34, 62].

Exergy model

Exergy analysis identifies the locations and magnitudes of thermodynamic irreversibilities throughout the SPT plant. The exergy associated with solar radiation incident on the receiver aperture is approximated as follows.

$$Ex_{solar} = Q_{incident} \times \left[1 - \frac{4}{3}\left(\frac{T_o}{T_{sun}}\right) + \frac{1}{3}\left(\frac{T_o}{T_{sun}}\right)^4\right]$$

where T_o is the ambient (dead-state) temperature, and T_{sun} is the effective blackbody temperature of the solar disc, approximately 5770 K [1, 22]. The exergy destruction in the receiver, the dominant irreversibility source in the SPT chain, arises primarily from heat transfer across large temperature differences between the concentrated solar flux and the receiver surface, and between the receiver surface and the HTF. It is expressed as:

$$Ex_{dest,receiver} = Ex_{solar,optical} - \left(Ex_{HTF,out} - Ex_{HTF,in}\right)$$

where the specific flow exergy of the HTF is given by:

$$Ex_{HTF} = \dot{m} \times \left[\left(h - h_o\right) - T_o\left(s - s_o\right)\right]$$

with h_o and s_o denoting the specific enthalpy and entropy at the dead state, respectively. The exergy efficiency of the receiver is accordingly defined as:

$$\psi_{receiver} = Ex_{HTF,out} / Ex_{solar,incident}$$

Reported values for the exergy efficiency of external tubular receivers operating with molten salt fall in the range of 0.65–0.8, with the dominant irreversibility attributed to the large temperature difference between the equivalent solar flux blackbody temperature, approximately 800–1000 °C at the receiver surface, and the salt exit temperature of approximately 565 °C [22, 25, 62]. Volumetric receivers, which achieve higher HTF exit temperatures and partially reduce this temperature mismatch, have the potential for higher exergy efficiency; however, quantitative comparative data for this configuration remain limited in the open literature. The exergy analysis framework described above can be applied to individual components or to the complete plant conversion chain, providing a rational thermodynamic basis for prioritizing design improvements and identifying the subsystems, receiver, TES heat exchanger, and power block condenser, where future research and development yield the greatest efficiency returns.

Contextualization of present findings against prior reviews

To situate the findings of the present review within the broader literature, it is instructive to compare its scope and conclusions with those of the most directly relevant prior reviews of SPT and CSP technology.

Behar et al. [22] presented a comprehensive review of central receiver SPT studies, covering receiver types, HTF selection, and power cycle options. The present work extends this foundation by incorporating recent developments, including the large-scale commercial deployment of molten salt SPT plants, Crescent Dunes, NOOR III, and DEWA, as well as the expanded operational database for DSG-SPT plants, including Ivanpah, Khi Solar One, and Ashalim. Importantly, the present review introduces the PHF metric as a practical, publicly computable performance index that enables a technology-neutral cross-fleet comparison, which was not available in [22].

Islam et al. [23] conducted a comprehensive state-of-the-art review of CSP technologies covering all four CSP configurations with emphasis on current status and research trends. That review identified SPT as the most promising technology for future large-scale deployment, a conclusion strongly reinforced by the present work's analysis of recent plant commissioning data, which reveals a clear market trend toward molten-salt SPT plants with large TES capacity in China, the Middle East, and Sub-Saharan Africa. While Islam et al. provided a foundational overview, this review extends their work by offering a comprehensive analysis of SPT-specific receiver physics, a comparative evaluation of HTF thermophysical properties, and a critical assessment of the DSG versus molten salt performance debate.

Merchán et al. [25] provided an overview of high-temperature SPT plants, focusing on thermodynamic cycles and component temperatures. The present review aligns with their conclusion that SPT technology is commercially mature for operating temperatures up to approximately 565 °C (the current molten salt limit) and that further performance improvement requires advances in HTF operating temperature, achievable through alternative salt formulations, solid particles, or high-temperature gases, and corresponding advances in receiver materials and TES technology. The present review extends the framework of Merchán et al. by adding an energy and exergy modelling framework and a discussion of design aspects applicable to new plant design and optimization.

Fundamental components of SPT

Heliostats field collectors (HFC)

Heliostats are formed from hundreds of flat or slightly curved mirrors with a focal displacement equal to the distance from the mirrors to the receiver. A computer controls the heliostats to ensure they always follow the sun as it moves across the sky. Unlike PTC and SPD, heliostats do not face the sun perpendicularly. Still, they evenly divide the angle between the incident solar flux direction and the heliostats-to-receiver pathway direction. Heliostats can be found in a range of geometries and sizes [35]. The standard size is quite large, up to 200 m^2, and manufactured from multiple mirrors constructed on the same support structure, while the small size is less than 1 m^2 and consists of a single mirror. Deploying this large number of heliostats results in a high concentration ratio and, consequently, a high thermal efficiency. Due to these thermodynamic advantages, steam turbines (Rankine cycle) and gas turbines (Brayton cycle) can be used in the conversion cycle.

Nevertheless, the criticality of these components can be summarized in terms of capital cost and optical efficiency. First, the capital cost of heliostats is quite high. Therefore, it plays a significant role in the plant's overall economic performance. It represents the lion's share (around 50%) of the total investment [36]. Therefore, tremendous efforts have been undertaken by R&D activities and researchers to minimize heliostat costs. Eventually, the cost dropped from 1000 USD m^{-2} to 150 USD m^{-2} [63]. Second, optical efficiency reduces the overall SPT efficiency; hence, the estimated annual thermal energy loss is around 50% [22]. Some key effects that reduce optical efficiency are: the overlapping effect (blocking and shading), the cosine effect, and the spillage effect due to increased optical aberrations around the receiver [60].

Receiver

It represents the heart of SPT plants, where solar thermal energy is intercepted and absorbed by the HTF. The receiver is where heat exchange occurs between the solar flux and the HTF. In receivers, the heat transfer fluid is either directly exposed to the radiation flux, as in volumetric and particle receivers, or indirectly exposed to it, as in external and cavity receivers. However, to further understand these solar receiver modules in terms of concept, design, function, and development, they are grouped into four receiver sets, as the current review demonstrates in detail.

External tubular receivers

A realistic example of this type is employed in the Solar One facility in California, USA. The receiver consists of multiple adjacent connected panels forming the cylindrical shape of the receiver [61] as shown in Fig. 3. Each panel comprises many vertically mounted tubes, often manufactured from stainless steel. Because of the significance of such components, it is mandatory to determine the number of tubes for each panel, the tube length and diameter, and the diameter of the receiver. Such factors significantly impact the thermal performance and efficiency of receivers. Eventually,

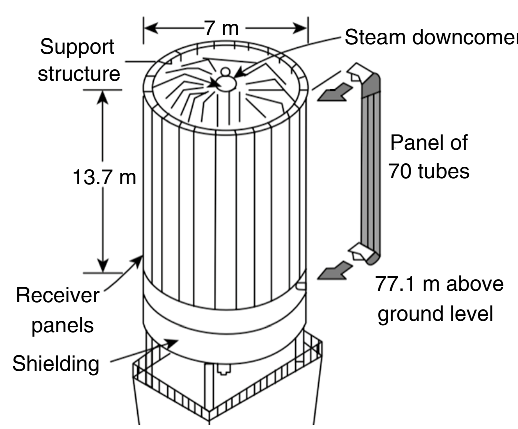

Fig. 3 A schematic of the external receiver of Solar One facility in the USA

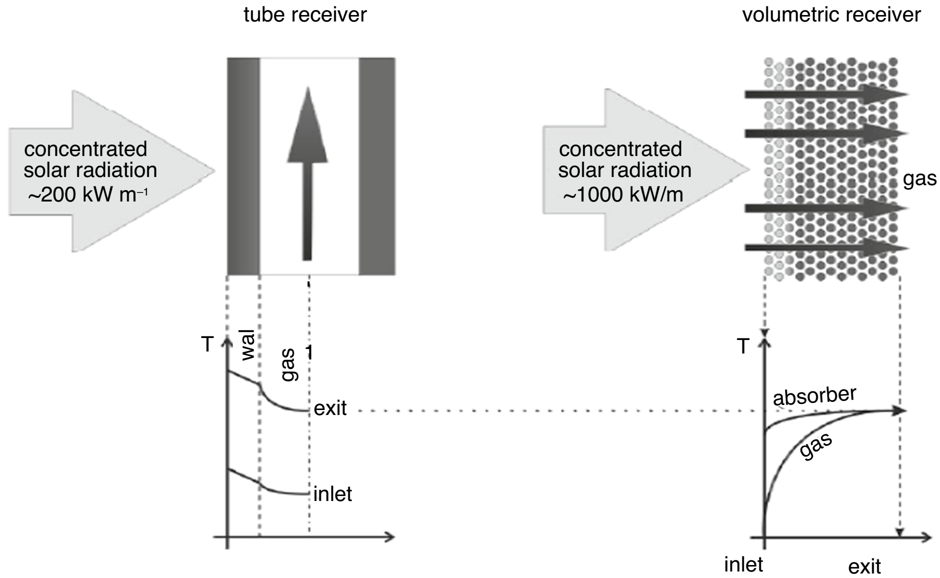

Fig. 4 Absorption comparison between the tubular and volumetric receivers

the amount of heat transferred to HTF is affected. The 7 m diameter solar receiver is composed of 24 panels; hence, each panel has 70 tubes. The tube's diameter and length are 12.7 mm and 13.7 m, respectively. The receiver efficiency is adversely affected by heat loss from external surfaces. Hence, heat loss to the atmosphere through convection, radiation, and reflection is a significant negative factor for the external receiver module. Also, receivers can absorb only a portion of the radiation reflected, while the rest is spillage. A larger receiver area results in greater absorbed radiation heat; however, it also helps minimize the concentration ratio. Indeed, it is recommended to minimize the surface area to the lowest possible limit. Even though tubular receivers have been used for a long time, the test report stated that the Solar One facility showed additional operational troubles, which can be briefly demonstrated below [61]:

- Deformation and overheating in the receiver part that is designed to form superheated steam because of solar thermal power transients and the weakness of heat transfer.
- After one and a half years of operation, leakages and cracks were found in the absorbing tubes.
- Huge temperature variation along the boiler tubes (edges and center) is detected. It is estimated to exceed 110 °C at the start and end of the operation.

Volumetric receivers

Unlike tubular external receivers, volumetric receivers have been under development for the past two decades and are composed of high-porosity materials, such as wires and foams [64]. These materials are made of either metals or ceramics. Heat exchange occurs within the receiver's volume, where HTF directly absorbs the radiated solar power inside the deep volume. The need to find a solar receiver with high thermal performance, cost-effectiveness, and simplicity has led to the development of volumetric receivers [65]. The best volumetric receivers exhibit a volumetric effect, in which the receiver side facing the solar irradiation has a lower temperature than the HTF exiting the receiver. Moreover, the volumetric receiver can deliver high working temperatures (over 1000 °C). The temperature distribution across the wall surface of tubular receivers and the manner in which concentrated solar power penetrates the porous face of volumetric receivers are illustrated in Fig. 4 [62]. Table 5 lists materials used in manufacturing volumetric receivers to achieve much higher exit temperatures. The latter would boost and maximize the thermodynamic efficiency of the solar thermal plant [66]. In operations-wise philosophy, flow rate stability and appropriate heat distribution are crucial and must be controlled. That would prevent operational problems such as cracking, overheating [67], and potential failure. When air passes through a porous structure, its density varies with temperature, altering the mass flow rate. In other words, the temperature increases, whereas density and

Table 5 Materials used in volumetric receivers result in high outlet temperatures [66]

Materials	Temperature range/°C	Status
Metals	800–1000	Achievable
SiSiC ceramics	1200	Achievable
SiC ceramics	1500	Achievable

mass flow rate decrease. This issue must be well addressed by controlling the mass flow rate, density, or exit temperature [68]. However, the literature indicates that stability could be achieved by using adequate receivers with high thermal conductivity, high viscous-to-inertia permeability coefficients, and high quadratic pressure drop [69]. Furthermore, this receiver can be classified by application, material, scheme, etc. However, this review will introduce two concepts regarding its exposure to ambient [70] as follows:

Open loop From the perspective of the power cycle used, the open-loop scheme operates in conjunction with the Rankine cycle to produce electric power. The air receives solar radiation as it passes through open-loop volumetric receivers, reaching nearly 700 °C. Then, the hot air exchanges energy with water in a heat recovery steam generator (HRSG) to produce steam. The thermodynamic properties of the steam are temperature (480–540 °C) and pressure (35–140 bar). The steam is directed to the power unit, which operates the conventional steam turbine and produces electricity. As stated earlier, this receiver is made of meshed-shaped metal wire. This scheme has been employed at the Phoebus-TSA plant, demonstrating several benefits for the HRSG return air. The enthalpy of the return air would be advantageous in enhancing receiver efficiency. In addition, such air would also cool down the receiver structure components [71].

Closed loop On the other hand, the closed-loop scheme works with the Brayton cycle. Hence, atmospheric air is compressed by a compressor and then heated to high temperatures by highly concentrated solar radiation. Then, hot, pressurized air can generate electricity via a gas turbine. However, such air is still carrying energy that could be exploited to boost cycle efficiency. HRSG extracts residual energy in the air to heat the water and generate additional steam for the Rankine cycle. The combined cycle (CC) (Brayton cycle and Rankine cycle) consolidated with SPT is beneficial in maximizing plant performance [72]. A combustor is also added to the gas turbine cycle to avoid intermittent solar energy on cloudy days and to attain stable dispatchability of electric power. The closed-loop volumetric receiver is veiled from the ambient by a glass window, permitting the irradiant power to enter the receiver volume. The REFOS volumetric receiver with a secondary concentrator, used to preheat air before introducing it to the combustor, is demonstrated in [57]. These modules have hexagonal apertures and are arranged in a honeycomb pattern to cover the overall area where the concentrated solar irradiance falls [73].

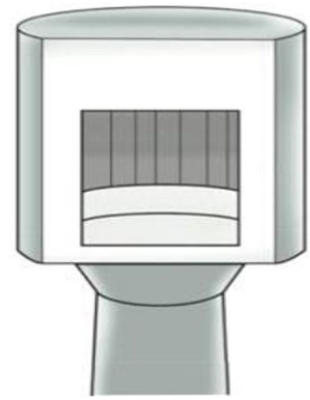

Fig. 5 A schematic of a cavity receiver

Cavity receiver

In the cavity receiver, the reflected irradiance from the heliostats enters the cavity through a so-called aperture into a box-like geometry before impinging on the absorber tubes, shown in Fig. 5. The cavity receiver can be used in large-capacity SPT plants or small-capacity SPD plants. High temperatures (over 400 °C) and decreasing thermal losses can be achieved by utilizing cavity receivers [74]. Natural convection is considered the primary heat-loss mechanism in the cavity receiver. Hence, the possibility of mass transfer through the aperture and of heating the atmospheric air inside the cavity embodies the two main parameters on which convective heat loss relies. Therefore, aperture orientation and characteristic length are critical aspects of cavity design. If the gaseous working fluid is used to operate the Brayton cycle, convective heat loss is much greater than with water/steam or molten salt because of the higher surface area required [75]. Table 6 summarizes scientists' and researchers' previous efforts, research, and contributions.

Material degradation in cavity receivers: mechanisms and mitigation strategies At the high operating temperatures characteristic of cavity receivers, routinely exceeding 400 °C at the absorber tube surface and reaching 600–800 °C or higher in advanced configurations, several material degradation mechanisms become operationally significant and must be addressed in both design and maintenance planning.

High-temperature oxidation is the first critical mechanism. Metallic absorber tubes exposed to air at elevated temperatures undergo progressive surface oxidation, forming oxide scales that reduce thermal conductivity, alter the optical absorptance of the selective coating, and in severe cases cause embrittlement and surface spalling. Stainless steels commonly used in cavity receivers, such as grades 316 SS and 347 SS, begin to exhibit significant oxidation above approximately 700 °C, while nickel-based superalloys,

Table 6 Main efforts and research undertaken on the cavity receiver

References	Contributions/conclusions
Harris and Lenz [74]	Found that five different geometry cavity receivers have a tremendous impact on the power profile and a negligible effect on the system efficiency
Zhilin et al. [76]	Presented an overview of a 70 kWe pressurized air cavity receiver, a demonstration solar tower project in China
Yu et al. [77]	Proposed an integrated model for the DAHAN power plant cavity receiver to simulate and test the dynamic characteristics of the specified receiver under abrupt solar intermittency. This model shows strong agreement with the design data. In addition, wind angle and velocity affect thermal losses
Fang et al. [37]	A combined calculation method approach was adopted to evaluate the cavity receiver's thermal performance. This method combines the Monte Carlo method (flow boiling correlations) with airflow calculations at various wind speeds. Surface heat flux, tube wall temperature, and heat loss were found. The maximum heat loss occurs when the wind is side-on
Yang et al. [78]	Used CFD software Fluent 6.2 to simulate and evaluate the temperature distributions, heat flux, and heat transfer characteristics in SPT with a molten salt tube receiver. They concluded that the temperature of the tube's inner surface is significant in protecting the molten salt from degradation. In addition, heat flux from the tube's outer surface increases as HTF velocity increases
Li et al. [79]	Developed a steady-state 100 kW thermal model of a molten salt cavity receiver for SPT in China. They studied the impact of the following parameters (emissivity, reflectivity, convection, number of tubes per panel, and tube diameter) on the receiver efficiency
Hinojosa et al. [80]	Studied and presented a horizontal-square-shape open cavity receiver in terms of natural convection and surface radiation
Chakroun et al. [81]	Performed experiments to evaluate the convective heat transfer coefficient for a tilted rectangular cavity receiver and the ambient
Gonzalez et al. [82]	Presented numerical computations for two heat transfer modes (natural convection and surface radiation) in 2D cavity receivers under high-temperature variations. Also, they found that high-temperature differences are more influential than convection
Paitoonsurikarn and Lovegrove [83]	A new correlation for the Nusselt number was presented, based on numerical results for three cavity receiver geometries
Dehghan and Behnia [84]	Performed a model in which the three heat transfer mechanisms (conduction, convection, radiation) are gathered in an open-top cavity receiver. They found that natural convection was the principal one
Kumar and Reddy [85]	A 2D model was presented to anticipate the natural convective loss from a cavity receiver, and the greatest loss was obtained when the receiver inclination was 0°
Taumoefolau et al. [86]	Investigated thermal loss by convection from an electrically-heated cavity receiver tilted from -90◦ to 90◦ and a temperature variation range of (450–650) °C. Their results and experimental data were in good agreement
Shirvan et al. [87]	Carried out numerical investigations on the surface thermal radiation coupled with natural convection for a square cavity receiver under fixed heat insolation
Ngo et al. [88]	Analyzed a 3D numerical model capturing heat loss mass inside the cavity receiver and optimized geometry parameters using the search algorithm. They found that natural convection inside the cavity receiver can be significantly reduced by using plate fins

including Inconel 625, Inconel 718, and Haynes 230, extend oxidation resistance to temperatures approaching 1050–1100 °C, providing a substantially wider operating margin [38, 61].

Creep and thermal fatigue represent the second category of degradation. Repeated thermal cycling associated with daily start-up and shutdown sequences and transient flux variations during cloud events imposes cyclic thermal stresses on absorber tube walls. These stresses are most severe at regions of peak heat flux and at geometric discontinuities such as tube-to-header welds and panel boundaries. Over thousands of operational cycles, creep deformation and low-cycle fatigue cracking progressively develop, ultimately leading to tube failure [26, 50, 89]. The creep-fatigue interaction is particularly damaging in thin-walled tubes operating near their allowable stress limits, as is the case in high-performance cavity receivers designed for maximum flux absorption.

Corrosion from HTF interaction is the third mechanism of concern. In molten-salt HTF, high-temperature corrosion of the inner tube wall is well documented. Nitrate salts are chemically aggressive towards carbon steels above approximately 450 °C and begin to attack stainless steel alloys above approximately 600 °C through a combination of general dissolution corrosion and stress corrosion cracking [34, 78]. Regular monitoring of salt chemistry, primarily water content and carbonate and chloride impurity levels, is essential to maintain corrosion rates within acceptable limits.

Selective coating degradation constitutes the fourth mechanism. High-absorptance selective coatings applied to absorber tubes, such as Pyromark 2500 high-temperature paint or physical vapor deposition (PVD) coatings, degrade under sustained high-temperature exposure and thermal cycling. Coating absorptance, initially in the range of 0.95–0.97, can decline by 0.02–0.05 over an operational season, directly reducing receiver thermal efficiency [38, 62]. Periodic recoating is therefore required as part of planned maintenance.

Mitigation strategies for these degradation mechanisms involve a combination of material selection, design of operating protocols, and structural monitoring. Material solutions include adopting nickel superalloys and oxide-dispersion-strengthened (ODS) alloys for the highest-temperature receiver zones, and applying ceramic thermal barrier coatings, alumina- or zirconia-based, as oxidation-protection layers on metallic substrates. Operational mitigation measures include controlled warm-up and cool-down ramp rates that limit the magnitude of the thermal gradient during transient events, and the avoidance of direct cold-fluid injection onto hot receiver surfaces following rapid cloud-induced flux reductions. Structural health monitoring using embedded thermocouples and acoustic emission sensors is increasingly incorporated into modern receiver designs, enabling early detection of developing fatigue cracks or corrosion-induced wall thinning and facilitating targeted maintenance interventions before catastrophic failure [50, 61, 78].

Particle receiver

The particle receiver, also called the falling particle receiver (FPR), is a new solar receiver technique with the potential to be integrated into various CSP technologies. This receiver can reach high operating temperatures, leading to greater efficiency and lower investment in thermal energy storage. Tiny solid particles are used to achieve two critical targets in SPT plants. First, these solid particles directly absorb reflected solar irradiance as they fall into the receiver. Second, such particles store thermal energy that will later be used to heat the power-cycle working fluid. In other words, there is no need for heat exchangers in the downstream field, as shown in Fig. 6 [38].

In the literature, some researchers, for instance, Tan and Chen [90], reviewed solid-particle SPT plants used to split water in a thermo-chemical process to produce hydrogen. They focused on the origins of this idea, its benefits and drawbacks, the fundamentals of design, and the theoretical design adopted by Sandia National Laboratories (SNL). However, other researchers have concentrated on numerical simulation, such as Grena et al. [91]. The latter provided a transient simulation model for the particle in a solar power particle receiver. They discovered that the particle's temperature distribution is not uniform due to particle size, rotation, and exposure time to irradiance. In addition, their results were consistent with the findings of Chen et al. [92]. Meier [93] has developed a CFD simulation of the coupling of radiation and convection heat transfer modes in falling particle receivers for a 1.5 MW-capacity cement plant. His findings were that if the particle diameter is less than 300 μm, it may be influenced by convection. Therefore, he advised using air

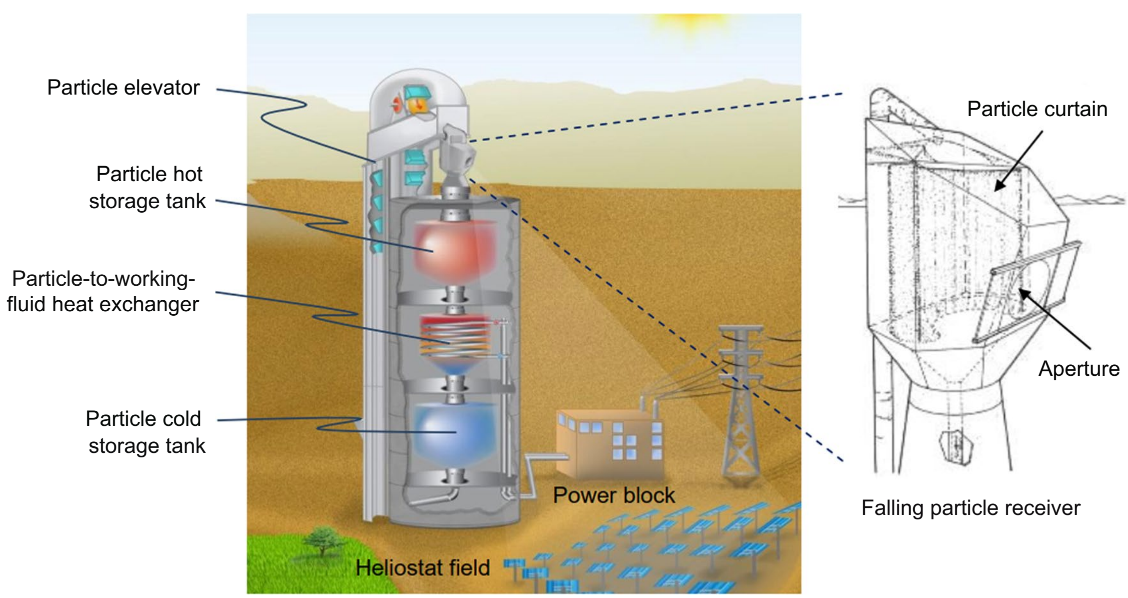

Fig. 6 An illustration of a particle receiver system

and translucent windows to mitigate the convection loss. Ho et al. [94] reported that a high-temperature (above 700 °C) 1 MW_{th} constantly recirculating falling-particle receiver was successfully utilized and tested at Sandia National Laboratories, New Mexico, USA. Also, they found that uniform insolation leads to uniform particle heating, with particles near the center having the largest magnitudes, whereas those near the edges have the smallest. Ho et al. [95] investigated two designs (obstructed flow particle and free-fall particle) of 1 MW falling particle receivers. The aim was to evaluate the effects of particle mass flow rate, insolation, and particle temperature on the particle temperature increment, as well as the thermal efficiency for each design of the solar receiver. Their results showed that the obstructed-flow-rate design extends particles' residence time, exposing them to concentrated solar flux. Consequently, particles' temperature and thermal efficiency increase as the flow rate increases. Kim et al. [96] developed a new particle receiver design model integrating a multi-stage falling concept, which is numerically and experimentally investigated via CFD simulation software. They reported several advantages of the new design: greater absorptivity, reduced unequal heating across particles' domains, and enhanced particle flow stability due to staged falling (Table 7).

Thermal energy storage (TES)

The thermal energy storage approach is a promising solution for storing thermal energy when the sun shines or when demand for electric power is low. The stored energy can then be used when the sun is fully/partially blocked by clouds, at night, or when demand for electric power is high. Such TES systems can bridge the gap between the solar energy supplied to SPT plants and the electricity demanded. TES plays a significant role in SPT plants; hence, it maintains the thermal load required for electric power generation during transient weather conditions. Thermal energy can be stored through various materials or techniques [97]. Current TES technologies are mainly classified as follows [98]:

1 Sensible heat thermal energy storage (SHTES) "lowest storage density."
2 Latent heat thermal energy storage (LHTES) "is higher than SHTES."
3 Chemical heat thermal energy storage (CHTES) "highest storage capacity."

TES concepts can be classified as active and passive. The active concept can be subdivided into two categories: direct and indirect. The whole tree of the TES materials is demonstrated in [99].

Sensible heat thermal energy storage is used in most commercial SPT plants worldwide. Different materials, such as rocks, sand, and oil, are used for that purpose. There is no phase change during charging and discharging. Such technology requires several thermally insulated tanks filled with TES materials to store thermal energy as a rise in temperature. In addition, sensible heat is stored in the liquid state, such as water, in the steam accumulator. The latter is integrated with SPT plants using direct steam generation. The steam accumulator is a pressurized vessel that adapts sensible heat storage technology to saturated liquid. For instance, the PS10 plant in Spain utilized a steam accumulator [100]. Although SHTES is a promising technology and has certain advantages, its drawbacks are the low storage density and high cost due to the high-pressure vessel investment [101]. Latent heat thermal energy storage can store several times as much energy as sensible heat thermal energy storage. Unlike SHTES, LHTES is based on phase change, and the materials used in this concept are called phase change materials (PCMs). The main disadvantage of such systems is, however, their low capability to transfer heat due to the poor thermal conductivity of most PCMs, resulting in modest rates of charging/discharging processes [102]. Even though research has been done to improve the heat transfer mechanism, there are still gaps in enhancing PCM performance at high temperatures. Chemical heat thermal energy storage occupies a prominent position among thermal storage concepts, in which a reversible chemical reaction stores and releases heat. However, this type of TES is still under development, and further research is required to implement it. In addition, because of the complexity of its unit design, thermochemical storage has not been utilized yet in any commercial SPT plants [25].

Comparative analysis of thermal energy storage technologies for SPT plants

While the three fundamental TES categories, sensible, latent, and thermochemical, were introduced in the preceding subsection, a structured comparative analysis is essential for evaluating their suitability in SPT applications. Table 8 presents a side-by-side comparison of the principal TES technologies based on operating temperature range, energy density, technology maturity, and key advantages and limitations.

The comparative analysis shows that the two-tank direct molten salt configuration is the only TES technology to have achieved full commercial deployment in large-scale SPT plants, combining adequate energy density with operational reliability and direct compatibility with the molten salt HTF circuit [25, 97, 98]. The single-tank thermocline configuration represents a cost-reduction pathway that uses the same storage medium, trading the simplicity of a single pressure vessel for the additional complexity of managing thermal

Table 7 Comparative analysis of solar receiver types used in SPT plants [61–96]

Receiver type	Operating temp. range/°C	Peak heat flux/kW m^{-2}	Compatible HTFs	Typical thermal efficiency	Key advantages/limitations	Technology maturity
External tubular	200–600	200–1000	Water /steam, molten salt, oil	85–90%	Proven technology; large-scale commercial experience; 360° heliostat geometry./High convective and radiative losses from exposed surface; thermal stress under non-uniform flux	Commercial
Cavity	400–1000	300–800	Water/steam, molten salt, pressurized gas	90–95%	Reduced convective and radiative losses due to enclosed geometry; higher efficiency at elevated temperature.Limited acceptance angle constrains heliostat field geometry	Commercial / Demonstration
Volumetric (open/closed)	700–> 1200	200–800	Air (open loop); pressurized gas (closed loop)	75–88%	Very high working temperatures; suitable for Brayton and combined cycles; the volumetric effect improves absorptance. / Flow instability; porous material durability; limited commercial experience	Pilot / Demonstration
Falling particle	> 700	400–> 1000	Solid particles (serve as direct storage)	80–90%	High operating temperature; particles serve as an integrated TES medium; eliminates the need for a downstream heat exchanger./Particle attrition and loss; convective losses at aperture; recirculation energy cost	Early Demonstration

Table 8 Comparative analysis of thermal energy storage technologies for SPT plant applications [25, 97]

TES type/configuration	Storage medium	Operating temp./°C	Energy density/kWh m^{-3}	Maturity	Key advantages/limitations	Commercial examples
Sensible, Two-tank direct	Molten salt (Solar Salt)	220–565	80–100	Commercial	High maturity; HTF doubles as TES medium; proven at large scale. / Freeze risk below 220 °C; high salt inventory cost	Gemasolar, Crescent Dunes, NOOR III
Sensible, Two-tank indirect	Molten salt+ separate HTF	290–565	60–80	Commercial (PTC-dominant)	Allows independent optimization of HTF and TES media /An additional heat exchanger adds cost and thermodynamic irreversibility	Andasol (PTC); limited SPT use
Sensible, Single-tank thermocline	Molten salt+ solid filler (rocks, quartz)	290–565	60–70	Demonstration	Lower cost than two-tank through a single vessel and filler material./Thermal stratification control; mixing losses during charge/discharge cycling	Solar Two (pilot); Sandia tests
Sensible, Steam accumulator	Saturated water/steam	180–230	15–30	Commercial	Simple integration with DSG plants./Very low energy density; storage duration typically below 1 h	PS10, PS20 (Spain)
Latent, PCM (high temperature)	Nitrate salts, metal alloys	150–800	100–300	R&D/Pilot	High energy density; near-isothermal discharge; reduced volume./ Low thermal conductivity; limited cycling durability at high temperature	No commercial SPT use to date
Thermochemical	Metal oxides, carbonates, hydroxides	> 200 (reaction-specific)	250–600	Early R&D	Highest theoretical energy density; potential for seasonal storage./ High system complexity; materials stability; not yet commercially deployed	Not yet commercial

stratification and its associated mixing losses during cyclic operation [98, 101]. Steam accumulators are well-suited to DSG plants but are fundamentally limited in storage duration to approximately 30–60 min at rated power, restricting their role to short-term buffering rather than hours-scale energy shifting [100, 101]. Latent heat and thermochemical storage technologies are the most promising candidates for the next generation of SPT plants, offering substantially higher energy densities and the potential for storage durations exceeding 15 h at reduced storage volume; however, both require further research and demonstration, particularly regarding high-temperature cycling durability and cost reduction, before commercial deployment in SPT systems becomes feasible [25, 98, 99, 102].

Power conversion block (Electricity generation unit)

It is the module where thermal energy from the solar receiver is converted into useful electric power by conventional steam or gas turbine engines. SPT power block employs one or more power conversion cycles (Brayton and Rankine cycles). The process begins by transforming thermal energy into mechanical energy, then into electrical power using a generator.

In the Brayton cycle, atmospheric air is pressurized by a compressor and flows toward the top of a tower where the solar receiver is located. Then, the compressed air will acquire thermal energy from the concentrated irradiance reflected by the heliostats. Then, it gains additional heat as it passes through the combustor, where its temperature exceeds 1000 °C [58]. Lastly, the hot, pressurized air performs useful work and produces electricity via the Brayton cycle in the gas turbine generator [59]. It is highly recommended that the distances between the compressor, receiver, and combustor be kept as short as possible to minimize losses in the connections. Even though hybridization integrates a fossil-fired combustor into solar-only SPT plants to maintain dispatchability around the clock when the sun is absent or overnight, this results in a decrease in compression ratio due to pressure losses and a reduction in overall performance. However, from an economic perspective, solar-only SPT plants significantly reduce fossil fuel use. It contributes to saving more than 2 million tons of fuel annually [59], and it has the potential to stand alone [103]. Moreover, the solarized gas turbine cycle, when combined with SPT, offers lower costs, higher efficiency, and more feasible land use than other CSP technologies [104].

The Rankine cycle, on the other hand, is very commonly used in CSP plants [60]. The basic concept is that HTF is supplied by the solar receiver and transfers heat to saturated water. Then, HTF will return to the solar receiver to collect the concentrated solar irradiance, and this cycle will be repeated. Water gaining thermal energy becomes superheated steam. The turbine will use high-temperature, high-pressure steam (around 550 °C and 60–100 bar) to convert thermal energy into electric power. Lastly, steam is condensed by rejecting heat to the surroundings and drawn by a saturated water pump. The capacity of steam turbines varies depending on the application. It ranges from several to hundreds of megawatts.

Hybridization is possible to minimize the amount of fossil fuel burned via boilers, and consequently, fewer greenhouse gas emissions [105]. The beauty of the power conversion cycles mentioned above is that they can be combined to form a combined-cycle (CC) system. In such a cycle, the effluent hot gases from the gas turbine still have heat, which could be used to increase the steam generated [22].

Potential research work

It is known that the main drive for SPT plants is solar thermal energy. The function of an SPT plant is to concentrate and reflect sun rays on the solar receiver to heat water and produce steam. The steam generated must meet the inlet turbine conditions (pressure, temperature, and enthalpy) to ensure continuous electricity dispatchability to the grid. However, such solar irradiance is intermittent due to cloud events and varies with the sun's position. Therefore, solar irradiance fluctuates throughout the diurnal cycle.

Many researchers investigated factors significantly impacting the SPT operational process and its subsystems. However, few publications have examined the effects of irradiance intermittency on SPT plants. For instance, Crespi et al. [106] presented a numerical model to evaluate the transient performance for a 19.9 MWe solar power tower plant utilizing molten salt and a thermal energy storage system under solar irradiance fluctuation due to cloud cover. They investigated the impacts of six different types of clouds on the tubular receiver's thermal performance. There are, however, further challenges that the next generation of SPT plants face, with some development prospects still open for improved performance of such plants, as follows [25]:

1. Heliostats
   - Further research is required to address the optimum dimensions, as the cost and optical efficiency play against each other.
   - An advanced method is needed to compute heliostats' performance with less computational cost.
2. Solar receiver
   - Research for higher efficiency of high-temperature solar receivers is still open for the following years.

- The use of a gaseous heat transfer fluid in an external receiver SPT could result in a more compact receiver, which means less cost required for construction materials, along with lower pressure drop.
- The volumetric receiver is still subject to the same challenges mentioned in using gaseous HTF.
- The particle receiver needs more investigation.
- Different designs and materials proposed for solar receivers should be tested under real weather conditions.

3. Thermal energy storage

- More reliable and efficient systems are needed to meet the SPT plant requirements.
- Molten salt TES could be further improved regarding temperature limits and optimization.
- Issues facing liquid metals and nanofluids, like cost and instability, need further investigation.

4. Power block

- More opportunities to improve the Brayton cycle are still available, but they should be tested thoroughly.
- As the combined cycle faces challenges like the Brayton cycle, it also involves promising prospects for further development.

Nevertheless, the impact of fluctuating irradiance on the receiver thermal performance requires more detailed analysis based on the high-resolution temporal change in solar irradiance [26, 89, 107]. Also, the effects of such solar fluctuations on the SPT subsystems still need further investigation. For example, thermal stresses and hotspots arising from changes in thermal load in the solar receiver are critical issues that should be carefully addressed to ensure system durability.

Advanced control strategies and artificial intelligence for SPT plant optimisation

The variable and intermittent nature of solar irradiance, driven by cloud transients, aerosol variability, and diurnal and seasonal cycles, presents a fundamental control challenge for SPT plants. Conventional proportional-integral-derivative (PID) control strategies designed for steady-state operation near fixed setpoints are inadequate for managing the wide, rapid dynamic range encountered by SPT subsystems, particularly the receiver and TES circuit. Advanced control frameworks and artificial intelligence (AI) techniques represent a high-potential research frontier for improving SPT operational efficiency, extending component service life, and enhancing grid integration capability.

Model predictive control (MPC) uses a mathematical dynamic model of the plant to anticipate future system states over a defined prediction horizon, typically 15 min to several hours, and to compute optimal control actions satisfying operating constraints while minimizing a cost function, usually combining energy output deviation, receiver thermal stress, and HTF temperature excursion. MPC has been demonstrated in simulation studies and limited experimental implementations for SPT receiver control, showing reductions in thermal stress events and improvements in net annual energy production of 2–5% relative to conventional PID control under variable irradiance conditions [106]. The primary implementation challenge is the need for an accurate, real-time-capable dynamic plant model and reliable short-horizon DNI forecasting input.

In terms of DSG-specific challenges, the two-phase flow behavior of water/steam within the receiver under variable irradiance introduces rapid oscillations in steam quality, pressure, and mass flow rate that are poorly managed by conventional control approaches. MPC architectures incorporating dynamic two-phase flow models of the receiver and its associated flow control valves have shown promise in simulation for stabilizing DSG receiver operation during cloud transients, maintaining steam outlet quality within acceptable bounds and avoiding pressure surge events. This application of advanced control to DSG-SPT systems is identified as a high-priority research area, given the large number of operational DSG-SPT plants and the demonstrated sensitivity of their performance to irradiance variability [26, 47, 89, 107].

Machine-learning-based solar resource forecasting is an enabling technology for any predictive control strategy. Accurate short-term DNI forecasting, with temporal resolutions of 1–10 min and spatial resolutions consistent with the plant's heliostat field extent, is essential for anticipating control actions before flux changes reach the receiver. Numerical weather prediction (NWP) models provide acceptable accuracy at 1–6-h horizons but are insufficiently resolved in time and space for minute-scale control. Machine learning approaches, including convolutional neural networks applied to all-sky imager time series, long short-term memory (LSTM) recurrent networks for time series extrapolation, and ensemble models combining physical and data-driven components, have demonstrated short-range forecast skill superior to persistence models at horizons of 1–30 min, which is precisely the control-relevant horizon for SPT receiver management [26, 89, 106, 107]. Research embedding such forecasting models within MPC frameworks for SPT plants is identified as an active and high-impact direction.

Reinforcement learning (RL) for heliostat field optimization represents a further emerging application. The real-time dispatching of individual heliostats, determining which mirrors to track, defocus, or redirect to alternative aim points on the receiver surface to achieve a desired flux distribution while avoiding hotspots, is a combinatorial optimization problem of very high dimensionality. RL agents trained in simulation environments representing the heliostat field optics and receiver thermal response have demonstrated the capability to learn near-optimal aiming strategies under variable irradiance conditions, including the ability to redistribute flux to thermally protect stressed receiver zones during high-irradiance events and to maximize energy delivery during partially overcast conditions [22, 60].

Finally, the development of digital twin frameworks for SPT plants, real-time, high-fidelity computational replicas continuously updated with sensor data, would provide operators with continuously updated plant performance predictions and early warning of developing component faults. An SPT digital twin integrating optical ray-tracing of the heliostat field, thermodynamic modelling of the receiver and power block, and degradation models for key components would enable condition-based rather than time-based maintenance, reducing unscheduled outages and extending component service intervals. The development and field validation of such frameworks are identified as a priority research objective that directly builds on the modelling foundations reviewed in Sect. "Energy and Exergy Analysis Framework for SPT Systems".

Conclusions and future perspectives

This review presents a comprehensive and structured examination of solar sower tower (SPT) technology, the most thermodynamically capable of the commercially mature concentrating solar power (CSP) configurations, with particular emphasis on the integration of direct steam generation (DSG), the comparative performance of heat transfer fluids, receiver component architectures, and thermal energy storage strategies. The following principal conclusions are drawn.

Key findings and scientific contributions

1. Thermodynamic Performance Metrics: The introduced Power-to-Heliostat-Field (PHF) metric effectively benchmarks operational SPT plants. DSG-based systems exhibit higher specific power outputs (87–159 W m^{-2}) than molten-salt plants (57–115 W m^{-2}) due to the high latent heat of vaporization of water. However, unbuffered DSG configurations suffer from low annual capacity factors (25–35%).
2. Commercial Dominance of Molten Salts: Two-tank direct molten salt TES remains the commercially dominant setup, enabling dispatchable baseload generation with capacity factors of 55–75%.
3. Thermal Limits of Receiver Architectures: External tubular receivers are constrained by material limits to operational thresholds around 565 °C. Conversely, volumetric and falling-particle designs demonstrate significant thermodynamic potential, with pilot-scale temperatures exceeding 1000 °C, thereby facilitating high-efficiency Brayton/combined-cycle operation.
4. TES Innovations: Commercial utility is restricted to sensible heat storage. High-energy–density alternatives, such as latent heat phase change materials (PCMs) and thermochemical TES, remain at the laboratory or pilot stage but are essential for achieving capacity factors near 80–90%.
5. Real-World Thermal Deficits: A significant performance gap exists between theoretical design points and real-world annual yields, with field data revealing energy deficits of 5–20%. These losses are primarily driven by unmodeled environmental off-design transient factors (e.g., cloud transients, localized tracking errors, and receiver soiling).

Limitations of the present work

The comparative PHF index relies on publicly available nameplate specifications rather than transient, measured operational data. Additionally, this study focuses strictly on utility-scale terrestrial power generation, omitting deep techno-economic modelling (LCOE) and emerging polygeneration applications (e.g., green hydrogen, industrial process heat) due to geographic and regulatory variability.

Future research directions

To bridge existing research gaps and facilitate the transition to next-generation solar thermal plants, the following research priorities are proposed:

- High-Resolution Transient Modelling: Developing advanced transient simulation tools validated against field data to model sub-minute thermal–hydraulic receiver responses. This is critical for predicting localized boiling instabilities in DSG loops, hotspot propagation, and thermal ratcheting in tube walls
- Advanced HTF and TES Materials: Formulating low-melting-point (< 100 °C) molten salts, specialized solid particles with optimized optical/thermophysical properties, and high-thermal-conductivity PCMs to break current thermodynamic limits
- Receiver Material Durability & Coatings: Conducting accelerated lifetime testing under coupled operational stressors, including severe thermal cycling, high-temperature oxidation, and molten-salt corrosion, to establish reliable degradation kinetics and predictive maintenance intervals.

- AI-Driven Predictive Flux Management: Integrating machine-learning-based direct normal irradiance (DNI) forecasting with model predictive control (MPC) and digital twin frameworks to optimize real-time receiver thermal management and mitigate transient thermal stresses.
- Empirical Environmental Correction: Establishing multi-site field measurement protocols to systematically quantify the impacts of soiling dynamics, wind-induced tracking errors, and dust deposition on receiver thermal efficiency.

In brief, while SPT technology is a commercially proven asset for deep grid decarbonization, addressing these material, thermodynamic, and control challenges would significantly decrease costs, elevate operating temperatures, and stabilize real-world performance predictability.

Author Contributions Conceptualization, H.A., A.A, and H.R.; methodology, H.A., and A.A.; investigation, A.A., and H.A.; resources, H.R., and H.A.; writing original draft preparation, H.A.; writing review and editing, A.A., and H.R.; visualization, H.A., A.A.; supervision, H.R. All authors have read and agreed to the published version of the manuscript.

Funding Open Access funding enabled and organized by CAUL and its Member Institutions.

Data Availability No datasets were generated or analysed during the current study.

Declarations

Conflict of interest The authors did not receive support from any organization for the submitted work. The authors declare they have no financial interests.

References

1. Rosen MA, Dincer I, Kanoglu M. Role of exergy in increasing efficiency and sustainability and reducing environmental impact. Energy Policy. 2008;36(1):128–37. https://doi.org/10.1016/j.enpol.2007.09.006.
2. Huang BN, Hwang MJ, Yang CW. Does more energy consumption bolster economic growth? An application of the nonlinear threshold regression model. Energy Policy. 2008;36(2):775–86. https://doi.org/10.1016/j.enpol.2007.11.002.
3. Raimi D, Campbell E, Newell RG, Prest B, Villanueva S, Wingenroth J "Global Energy Outlook 2022: Turning Points and Tension in the Energy Transition," 2022.
4. Rout UK, Akimoto K, Sano F, Oda J, Homma T, Tomoda T. Impact assessment of the increase in fossil fuel prices on the global energy system, with and without CO_2 concentration stabilization. Energy Policy. 2008;36(9):3477–84. https://doi.org/10.1016/j.enpol.2008.05.030.
5. Alrikabi N. Renewable energy types. J Clean Energy Technol. 2014;2(1):61–4. https://doi.org/10.7763/jocet.2014.v2.92.
6. Armin M, Gholinia M, Pourfallah M, Ranjbar AA. Investigation of the fuel injection angle/time on combustion, energy, and emissions of a heavy-duty dual-fuel diesel engine with reactivity control compression ignition mode. Energy Rep. 2021;7:5239–47. https://doi.org/10.1016/j.egyr.2021.08.115.
7. Mekhilef S, Saidur R, Safari A. A review on solar energy use in industries. Renew Sustain Energy Rev. 2011;15(4):1777–90. https://doi.org/10.1016/j.rser.2010.12.018.
8. Nejat P, Jomehzadeh F, Taheri MM, Gohari M, Muhd MZ. A global review of energy consumption, CO_2 emissions and policy in the residential sector (with an overview of the top ten CO_2 emitting countries). Renew Sustain Energy Rev. 2015;43:843–62. https://doi.org/10.1016/j.rser.2014.11.066.
9. Al-Kayiem HH, Mohammad ST. Potential of renewable energy resources with an emphasis on solar power in Iraq: an outlook. Resources (Basel). 2019;8(42):1–20. https://doi.org/10.3390/resources8010042.
10. Alhusseny A, Al-Zurfi N, Nasser A, Al-Fatlawi A, Aljanabi M. Impact of using a PCM-metal foam composite on charging/discharging process of bundled-tube LHTES units. Int J Heat Mass Transf. 2020. https://doi.org/10.1016/j.ijheatmasstransfer.2020.119320.
11. Belgasim B, Aldali Y, Abdunnabi MJR, Hashem G, Hossin K. The potential of concentrating solar power (CSP) for electricity generation in Libya. Renew Sustain Energy Rev. 2018;90(March):1–15. https://doi.org/10.1016/j.rser.2018.03.045.
12. Rogers JW, Louis GE. Method for comparative performance assessment and evaluation of consolidating community water systems as a regional water system. J Infrastruct Syst. 2007;13(4):280–6. https://doi.org/10.1061/(asce)1076-0342(2007)13:4(280).
13. Islam MT, Shahir SA, Uddin TMI, Saifullah AZA. Current energy scenario and future prospect of renewable energy in Bangladesh. Renew Sustain Energy Rev. 2014;39:1074–88. https://doi.org/10.1016/j.rser.2014.07.149.
14. Panwar NL, Kaushik SC, Kothari S. Role of renewable energy sources in environmental protection: a review. Renew Sustain Energy Rev. 2011;15(3):1513–24. https://doi.org/10.1016/j.rser.2010.11.037.
15. Khandouzi O, Pourfallah M, Yoosefirad E, Shaker B, Gholinia M, Mouloodi S. Evaluating and optimizing the geometry of thermal foundation pipes for the utilization of the geothermal energy: numerical simulation. J Energy Storage. 2021;37:102464. https://doi.org/10.1016/j.est.2021.102464.
16. Aringhoff R, Brakmann G, Geyer M, Teske S (2005) "EXPLOITING THE HEAT FROM THE SUN TO COMBAT CLIMATE CHANGE CONCENTRATED SOLAR THERMAL POWER," Hamburg.
17. Mathur A, Agrawal GD, Chandel M. Techno-economic analysis of solar parabolic trough type energy system for garment zone of

Jaipur city. Renew Sustain Energy Rev. 2013;17:104–9. https://doi.org/10.1016/j.rser.2012.09.015.
18. Gupta PK. Renewable energy sources-a longway to go in India. Renew Energy. 1999;16:1216–9. https://doi.org/10.1016/S0960-1481(98)00486-8.
19. Tian Y, Zhao CY. A review of solar collectors and thermal energy storage in solar thermal applications. Appl Energy. 2013;104:538–53. https://doi.org/10.1016/j.apenergy.2012.11.051.
20. Belgasim B, Aldali Y. Review on solar thermal electricity in Libya. Sol Energy Sustain Dev. 2018;7:49–60. https://doi.org/10.51646/jsesd.v7iSI.74.
21. Beust C, Franquet E, Bédécarrats JP, Garcia P. A numerical investigation of some key factors for the simulation of convection-dominated melting. Int J Therm Sci. 2021. https://doi.org/10.1016/j.ijthermalsci.2020.106687.
22. Behar O, Khellaf A, Mohammedi K. A review of studies on central receiver solar thermal power plants. Renew Sustain Energy Rev. 2013;23:12–39. https://doi.org/10.1016/j.rser.2013.02.017.
23. Islam MT, Huda N, Abdullah AB, Saidur R. A comprehensive review of state-of-the-art concentrating solar power (CSP) technologies: current status and research trends. Renew Sustain Energy Rev. 2018;91:987–1018. https://doi.org/10.1016/j.rser.2018.04.097.
24. Kuravi S, Trahan J, Goswami DY, Rahman MM, Stefanakos EK. Thermal energy storage technologies and systems for concentrating solar power plants. Prog Energy Combust Sci. 2013;39(4):285–319. https://doi.org/10.1016/j.pecs.2013.02.001.
25. Merchán RP, Santos MJ, Medina A, CalvoHernández A. High temperature central tower plants for concentrated solar power: 2021 overview. Renew Sustain Energy Rev. 2022;155:111828. https://doi.org/10.1016/j.rser.2021.111828.
26. Al-sarraf H, Alhusseny A, Zamora R."Impact of Weather Conditions Variability on External Receivers in Real-world Direct Steam Generation Solar Power Tower Plants," J Therm Sci Eng Appl. 2025 1–35
27. Elmaddah E. "An Assessment of Concentrating Solar Power for Egyptian Locations," Auckland University of Technology, 2018.
28. Braun FG, Hooper E, Wand R, Zloczysti P. Holding a candle to innovation in concentrating solar power technologies: a study drawing on patent data. Energy Policy. 2011;39(5):2441–56. https://doi.org/10.1016/j.enpol.2011.02.008.
29. Ummel K, Wheeler D. "Desert Power: The Economics of Solar Thermal Electricity for Europe, North Africa, and the Middle East," Cent Glob Dev. 2008;156.
30. Damerau K, Williges K, Patt AG, Gauché P. Costs of reducing water use of concentrating solar power to sustainable levels: scenarios for North Africa. Energy Policy. 2011;39(7):4391–8. https://doi.org/10.1016/j.enpol.2011.04.059.
31. Ortiz-Rivera EI, Feliciano-Cruz LI. "Performance evaluation and simulation of a Solar Thermal Power Plant", in 2009 IEEE Energy Conversion Congress and Exposition. ECCE. 2009;2009:337–44. https://doi.org/10.1109/ECCE.2009.5316215.
32. Sharma C, Sharma AK, Mullick SC, Kandpal TC. Assessment of solar thermal power generation potential in India. Renew Sustain Energy Rev. 2015;42:902–12. https://doi.org/10.1016/j.rser.2014.10.059.
33. Ummadisingu A, Soni MS. Concentrating solar power - technology, potential and policy in India. Renew Sustain Energy Rev. 2011;15(9):5169–75. https://doi.org/10.1016/j.rser.2011.07.040.
34. N. R. E. L. (NREL), "Concentrating Solar Power Projects: Power Tower Projects." https://solarpaces.nrel.gov/by-technology/power-tower (accessed Feb. 01, 2023).
35. Kolb GJ, et al. "Heliostat Cost Reduction Study Gregory", California. USA. 2007. https://doi.org/10.1115/ES2007-36217.
36. Fadlallah SO. "Lightweight composite structure for solar central receiver heliostats," Auckland University of Technology, 2020.
37. Fang JB, Wei JJ, Dong XW, Wang YS. Thermal performance simulation of a solar cavity receiver under windy conditions. Sol Energy. 2011;85(1):126–38. https://doi.org/10.1016/j.solener.2010.10.013.
38. Ho C, et al. Technology advancements for next generation falling particle receivers. Energy Procedia. 2014;49:398–407. https://doi.org/10.1016/j.egypro.2014.03.043.
39. Pitz-Paal R, Dersch J, Milow B. European concentrated solar thermal road-mapping (ECOSTAR). Germany: Cologne; 2005.
40. Pavlović TM, Radonjić IS, Milosavljević DD, Pantić LS. A review of concentrating solar power plants in the world and their potential use in Serbia. Renew Sustain Energy Rev. 2012;16(6):3891–902. https://doi.org/10.1016/j.rser.2012.03.042.
41. Romero M, Steinfeld A. Concentrating solar thermal power and thermochemical fuels. Energy Environ Sci. 2012;5(11):9234–45. https://doi.org/10.1039/c2ee21275g.
42. Kalogirou SA. Solar Energy Engineering Processes and Systems. 2nd ed. USA: San Diego; 2014.
43. Luo Y, Du X, Yang L, Xu C, Amjad M. Impacts of solar multiple on the performance of direct steam generation solar power tower plant with integrated thermal storage. Front Energy. 2017;11(4):461–71. https://doi.org/10.1007/s11708-017-0503-5.
44. Alhayek B, Agelin-Chaab M, Reddy B. Analysis of an innovative direct steam generation-based parabolic trough collector plant hybridized with a biomass boiler. Int J Energy Res. 2017;41(14):2236–47. https://doi.org/10.1002/er.3785.
45. Pramanik S, Ravikrishna RV. A review of concentrated solar power hybrid technologies. Appl Therm Eng. 2017;127:602–37. https://doi.org/10.1016/j.applthermaleng.2017.08.038.
46. Mokhtar M, Berger M, Zahler C, Krüger D, Schenk H, Stieglitz R. Direct steam generation for process heat using Fresnel collectors. Int J Therm Environ Eng. 2015;10(1):3–9. https://doi.org/10.5383/ijtee.10.01.001.
47. Boretti A, Castelletto S, Al-Zubaidy S. Concentrating solar power tower technology: present status and outlook. Nonlinear Eng. 2019;8(1):10–31. https://doi.org/10.1515/nleng-2017-0171.
48. Zhang HL, Baeyens J, Degrève J, Cacères G. Concentrated solar power plants: review and design methodology. Renew Sustain Energy Rev. 2013;22:466–81. https://doi.org/10.1016/j.rser.2013.01.032.
49. Manente G, Rech S, Lazzaretto A. Optimum choice and placement of concentrating solar power technologies in integrated solar combined cycle systems. Renew Energy. 2016;96:172–89. https://doi.org/10.1016/j.renene.2016.04.066.
50. Pang L, Wang T, Li R, Yang Y. Two-stage solar power tower cavity-receiver design and thermal performance analysis. AIP Conf Proc. 2017;1850:030037. https://doi.org/10.1063/1.4984380.
51. Pitz-Paal R. Concentrating solar power. In: Letcher T, editor. Futute energy: improved, sustainable and clean options for our planet. 1st ed. Elsevier Ltd.; 2008. p. 171–92.
52. Radosevich LG, Skinrood AC. The power production operation of solar one, the 10 mwe solar thermal central receiver pilot plant1. J Sol Energy Eng Trans ASME. 1989;111(2):144–51. https://doi.org/10.1115/1.3268300.
53. Kalogirou SA. Solar thermoelectric power generation in Cyprus: selection of the best system. Renew Energy. 2013;49:278–81. https://doi.org/10.1016/j.renene.2012.01.014.

54. Kalogirou SA. Seawater desalination using renewable energy sources. Prog Energy Combust Sci. 2005;31(3):242–81. https://doi.org/10.1016/j.pecs.2005.03.001.
55. Villafán-Vidales HI, Abanades S, Caliot C, Romero-Paredes H. Heat transfer simulation in a thermochemical solar reactor based on a volumetric porous receiver. Appl Therm Eng. 2011;31(16):3377–86. https://doi.org/10.1016/j.applthermaleng.2011.06.022.
56. Alexopoulos S, Hoffschmidt B. Solar tower power plant in Germany and future perspectives of the development of the technology in Greece and Cyprus. Renew Energy. 2010;35(7):1352–6. https://doi.org/10.1016/j.renene.2009.11.003.
57. Parzen M. Comparison of Heat Transfer Fluids (HTF) for Solar Tower Systems. Germany: University of Applied Sciences Nuremberg; 2017.
58. Heller P, et al. Test and evaluation of a solar powered gas turbine system. Sol Energy. 2006;80(10):1225–30. https://doi.org/10.1016/j.solener.2005.04.020.
59. Behar O, Abdallah K, Kamal M. “Scaling up Solar Hybrid Gas Turbine Electric Power System: Simulation and Results.”
60. Ginley DS, Cahen D, editors. Fundamentals of materials for energy and environmental sustainability. 1st ed. Cambridge: Cambridge University Press; 2012.
61. Goswami DY, Kreith F, editors. Energy conversion. 2nd ed. Boca Rato, Florida: CRC Press, Taylor & Francis Group; 2017.
62. Romero M, Buck R, Pacheco JE. An update on solar central receiver systems, projects, and technologies. J Sol Energy Eng Trans ASME. 2002;124(2):98–108. https://doi.org/10.1115/1.1467921.
63. Nixon JD, Dey PK, Davies PA. Which is the best solar thermal collection technology for electricity generation in north-west India? Evaluation of options using the analytical hierarchy process. Energy. 2010;35(12):5230–40. https://doi.org/10.1016/j.energy.2010.07.042.
64. Fend T, Hoffschmidt B, Pitz-Paal R, Reutter O, Rietbrock P. Porous materials as open volumetric solar receivers: experimental determination of thermophysical and heat transfer properties. Energy. 2004;29(5–6):823–33. https://doi.org/10.1016/S0360-5442(03)00188-9.
65. He YL, Cheng ZD, Cui FQ, Li ZY, Li D. Numerical investigations on a pressurized volumetric receiver: solar concentrating and collecting modelling. Renew Energy. 2012;44:368–79. https://doi.org/10.1016/j.renene.2012.02.001.
66. Sani E, Mercatelli L, Francini F, Sans JL, Sciti D. Ultra-refractory ceramics for high-temperature solar absorbers. Scr Mater. 2011;65(9):775–8. https://doi.org/10.1016/j.scriptamat.2011.07.033.
67. García-Martín FJ, Berenguel M, Valverde A, Camacho EF. Heuristic knowledge-based heliostat field control for the optimization of the temperature distribution in a volumetric receiver. Sol Energy. 1999;66(5):355–69. https://doi.org/10.1016/S0038-092X(99)00024-9.
68. Kribus A, Ries H, Spirkl W. Inherent limitations of volumetric solar receivers. J Sol Energy Eng Trans ASME. 1996;118(3):151–5. https://doi.org/10.1115/1.2870891.
69. Becker M, et al. Theoretical and numerical investigation of flow stability in porous materials applied as volumetric solar receivers. Sol Energy. 2006;80(10):1241–8. https://doi.org/10.1016/j.solener.2005.11.006.
70. Ávila-Marín AL. Volumetric receivers in solar thermal power plants with central receiver system technology: a review. Sol Energy. 2011;85(5):891–910. https://doi.org/10.1016/j.solener.2011.02.002.
71. Marcos MJ, Romero M, Palero S. Analysis of air return alternatives for CRS-type open volumetric reciever. Energy. 2004;29(5–6):677–86. https://doi.org/10.1016/S0360-5442(03)00176-2.
72. Buck R, Abele M, Kunberger J, Denk T, Heller P, Lüpfert E. Receiver for solar-hybrid gas turbine and combined cycle systems. J Phys Arch. 1999;9(3):537–44. https://doi.org/10.1051/jp4:1999385.
73. Buck R, Bräuning T, Denk T, Pfänder M, Schwarzbözl P, Tellez F. Solar-hybrid gas turbine-based power tower systems (REFOS). J Sol Energy Eng Trans ASME. 2002;124(1):2–9. https://doi.org/10.1115/1.1445444.
74. Harris JA, Lenz TG. Thermal performance of solar concentrator/cavity receiver systems. Sol Energy. 1985;34(2):135–42. https://doi.org/10.1016/0038-092X(85)90170-7.
75. Clausing AM. An analysis of convective losses from cavity solar central receivers. Sol Energy. 1981;27(4):295–300. https://doi.org/10.1016/0038-092X(81)90062-1.
76. Zhilin F, Yaoming Z, Deyou L, Jun W, Wei L. “Discussion of mechanical design for pressured cavity-air-receiver in solar power tower system”, in ISES Solar World Congress 2007. ISES. 2007;2007:1868–72. https://doi.org/10.1007/978-3-540-75997-3_381.
77. Yu Q, Wang Z, Xu E. Simulation and analysis of the central cavity receiver’s performance of solar thermal power tower plant. Sol Energy. 2012;86(1):164–74. https://doi.org/10.1016/j.solener.2011.09.022.
78. Yang X, Yang X, Ding J, Shao Y, Fan H. Numerical simulation study on the heat transfer characteristics of the tube receiver of the solar thermal power tower. Appl Energy. 2012;90(1):142–7. https://doi.org/10.1016/j.apenergy.2011.07.006.
79. Li X, Kong W, Wang Z, Chang C, Bai F. Thermal model and thermodynamic performance of molten salt cavity receiver. Renew Energy. 2010;35(5):981–8. https://doi.org/10.1016/j.renene.2009.11.017.
80. Hinojosa JF, Estrada CA, Cabanillas RE, Alvarez G. Numerical study of transient and steady-state natural convection and surface thermal radiation in a horizontal square open cavity. Numer Heat Transf Part A Appl. 2005;48(2):179–96. https://doi.org/10.1080/10407780590948936.
81. Chakroun W, Elsayed MM, Al-Fahed SF. Experimental measurements of heat transfer coefficient in a partially/fully opened tilted cavity. J Sol Energy Eng. 1997;119:298–303.
82. Montiel Gonzalez M, Hinojosa Palafox J, Estrada CA. Numerical study of heat transfer by natural convection and surface thermal radiation in an open cavity receiver. Sol Energy. 2012;86(4):1118–28. https://doi.org/10.1016/j.solener.2012.01.005.
83. Paitoonsurikarn Lovegrove S. “A new correlation for predicting the free convection loss from solar dish concentrating receivers,” In: Proceedings of the 44th Conference of the Australia and New Zealand Solar Energy Society (ANZSES), 2006, pp. 1–9.
84. Dehghan AA, Behnia M. Combined natural convection-conduction and radiation heat transfer in a discretely heated open cavity. J Heat Transf. 1996;118(1):56–64. https://doi.org/10.1115/1.2824068.
85. Sendhil Kumar N, Reddy KS. Numerical investigation of natural convection heat loss in modified cavity receiver for fuzzy focal solar dish concentrator. Sol Energy. 2007;81(7):846–55. https://doi.org/10.1016/j.solener.2006.11.008.
86. Taumoefolau T, Paitoonsurikarn S, Hughes G, Lovegrove K. Experimental investigation of natural convection heat loss from a model solar concentrator cavity receiver. J Sol Energy Eng Trans ASME. 2004;126(2):801–7. https://doi.org/10.1115/1.1687403.
87. Shirvan KM, Mamourian M, Mirzakhanlari S, Rahimi AB, Ellahi R. Numerical study of surface radiation and combined natural convection heat transfer in a solar cavity receiver. Int J Numer

Methods Heat Fluid Flow. 2017;27(10):2385–99. https://doi.org/10.1108/HFF-10-2016-0419.

88. Ngo LC, Bello-Ochende T, Meyer JP. Numerical modelling and optimisation of natural convection heat loss suppression in a solar cavity receiver with plate fins. Renew Energy. 2015;74:95–105. https://doi.org/10.1016/j.renene.2014.07.047.
89. Al-Sarraf H, Alhusseny A, Zamora R. "Solar Power Tower Plants Considering Meteorological Dynamics - Safety and Reliability Optimization," In: *2025 IEEE PES 17th Asia-Pacific Power and Energy Engineering Conference (APPEEC)*, 2026, pp. 1–5, https://doi.org/10.1109/APPEEC66370.2025.11382077.
90. Tan T, Chen Y. Review of study on solid particle solar receivers. Renew Sustain Energy Rev. 2010;14(1):265–76. https://doi.org/10.1016/j.rser.2009.05.012.
91. Grena R. Thermal simulation of a single particle in a falling-particle solar receiver. Sol Energy. 2009;83(8):1186–99. https://doi.org/10.1016/j.solener.2009.02.001.
92. Chen H, Chen Y, Hsieh HT, Siegel N. Computational fluid dynamics modeling of gas-particle flow within a solid-particle solar receiver. J Sol Energy Eng Trans ASME. 2007;129(2):160–70. https://doi.org/10.1115/1.2716418.
93. Meier A. A predictive CFD model for a falling particle receiver/reactor exposed to concentrated sunlight. Chem Eng Sci. 1999;54(13–14):2899–905. https://doi.org/10.1016/S0009-2509(98)00376-5.
94. Ho CK, et al. "On-sun testing of an advanced falling particle receiver system", SolarPACES 2015. AIP Conf Proc. 2016;1734(030022):1–8. https://doi.org/10.1063/1.4949074.
95. Ho CK et al. "Performance evaluation of a high-temperature falling particle receiver," In: Proceedings of the ASME 2016 10th International Conference on Energy Sustainability (ES2016), 2016, vol. ES2016–592, pp. 1–8, https://doi.org/10.1115/ES2016-59238.
96. Kim JS, Kumar A, Gardner W, Lipiński W. "Numerical and experimental investigation of a novel multi-stage falling particle receiver", SolarPACES 2018. AIP Conf Proc. 2019;2126(030030):1–8. https://doi.org/10.1063/1.5117542.
97. Herrmann U, Kearney DW. Survey of thermal energy storage for parabolic trough power plants. J Sol Energy Eng Trans ASME. 2002;124(2):145–52. https://doi.org/10.1115/1.1467601.
98. Medrano M, Gil A, Martorell I, Potau X, Cabeza LF. State of the art on high-temperature thermal energy storage for power generation. Part 2-case studies. Renew Sustain Energy Rev. 2010;14(1):56–72. https://doi.org/10.1016/j.rser.2009.07.036.
99. Nazir H, et al. Recent developments in phase change materials for energy storage applications: a review. Int J Heat Mass Transf. 2019;129:491–523. https://doi.org/10.1016/j.ijheatmasstransfer.2018.09.126.
100. Osuna R et al. "PS10, Construction of a 11MW solar thermal tower plant in Seville, Spain," In: 13th International Symposium on Concentrated Solar Power and Chemical Energy Technologies, 2006, no. 20th June, pp. 20–23.
101. Prieto C, Rodríguez A, Patiño D, Cabeza LF. Thermal energy storage evaluation in direct steam generation solar plants. Sol Energy. 2018;159(December 2017):501–9. https://doi.org/10.1016/j.solener.2017.11.006.
102. Hale DV, Hoover MJ,'Neill MJO. "Phase Change Materials Handbook," Huntsville, Alabama, 1971.
103. Dickey B. "Test results from a concentrated solar microturbine Brayton cycle integration," In: Proceedings of ASME Turbo Expo 2011 (GT2011), pp. 45918–1–45918–6.
104. Sinai J, Sugarmen C, Fisher U. "Adaptation and modification of gas turbines for solar energy applications," In: Proceedings of GT2005 ASME Turbo Expo 2005: Power for Land, Sea and Air, pp. 68122–1–68122–8.
105. Yang Q, Chen GQ, Zhao YH, Chen B, Li Z, Wang ZF. Energy cost and greenhouse gas emissions of a Chinese solar tower power plant. Procedia Environ Sci. 2011;5:77–80. https://doi.org/10.1016/j.proenv.2011.03.051.
106. Crespi F, Toscani A, Zani P, Sánchez D, Manzolini G. Effect of passing clouds on the dynamic performance of a CSP tower receiver with molten salt heat storage. Appl Energy. 2018;229(July):224–35. https://doi.org/10.1016/j.apenergy.2018.07.094.
107. Al-Sarraf H, Alhusseny A, Zamora R. A novel transient thermal analysis of direct steam generation external receivers in solar power tower plants under atmospheric conditions fluctuations. J Therm Sci Eng Appl. 2026. https://doi.org/10.1115/1.4071795.